Title
Electrodeposited Transition Metal Oxides as Electrocatalysts for Methane Partial Oxidation

Author
Huang, Yu-Chao

Publication Date
2021

Peer reviewed|Thesis/dissertation

UNIVERSITY OF CALIFORNIA

Los Angeles

Electrodeposited Transition Metal Oxides as Electrocatalysts for Methane Partial Oxidation

A thesis submitted in partial satisfaction

of the requirements for the degree Master of Science

in Chemical Engineering

by

Yu-Chao Huang

2021

ABSTRACT OF THE THESIS

Electrodeposited Transition Metal Oxides as Electrocatalysts

for Methane Partial Oxidation

by

Yu-Chao Huang

Master of Science in Chemical Engineering

University of California, Los Angeles, 2021

Professor Philippe Sautet, Chair

The conversion of methane to valuable chemicals via electrochemical approaches is of great interest in the field of catalysis. Conventional catalytic processes utilize extreme conditions (high temperatures or pressures) to provide the energy required to achieve methane activation and require sophisticated heat integration networks to be economically viable. In contrast, catalytic processes via electrification or electrocatalysis offers direct routes of methane activation under ambient conditions, with lower energy requirements and simplified configurations. However, electrochemical oxidation of methane using current electrocatalysts remains challenging due to low energy efficiencies and a seemingly unavoidable trade-off between conversion and selectivity.

In this regard, many research efforts have been devoted to the development of efficient and selective electrocatalysts for the activating and transformation of methane into valuable chemicals.

Over the last decade, researchers have shown that composite transition metal oxides such as NiO/ZrO_2 and Co_3O_4/ZrO_2 can catalyze the electrochemical partial oxidation of methane to value-added chemicals such as methanol, ethanol, and propanol in a carbonate electrolyte. Chemical co-precipitation has been utilized predominantly for the preparation of metal oxide catalysts which involves multiple steps such as centrifugation, collection, drying, and annealing, and result in oxide materials with poor conductivity which are not amenable to electrocatalysis. In this work, a one-step electrodeposition method has been developed for the preparation of $CoZrO_x$ electrocatalysts. The electrodeposited $CoZrO_x$ material was found to be an active electrocatalyst for the partial oxidation of methane with a simple fabrication method. Furthermore, different electrodeposited unary transition metal oxides (CoO_x, NiO_x, MnO_x, FeO_x, and CuO_x) were prepared through the same electrodeposition method, and were also studied for the electrochemical oxidation of methane. CoO_x, NiO_x, CuO_x, and the $CoZrO_x$ electrocatalysts have been discovered to catalyze the conversion of methane to methanol. The preliminary results in this work demonstrate an additional approach among the available strategies for catalyst fabrication and may provide an efficient strategy of catalyst preparation for further studies of the electrochemical oxidation of methane under ambient conditions.

The thesis of Yu-Chao Huang is approved.

Carlos G. Morales-Guio

Dante A Simonetti

Yunfeng Lu

Philippe Sautet, Committee Chair

University of California, Los Angeles

2021

Table of content

List of figures

List of tables

Acknowledgements

Studying at UCLA has been one of the most amazing journeys in my life. As a graduate student here, I have the privilege of working in an incredible academic education and research environment, for which I would like to express my sincere gratitude to the following individuals who have made this academic journey possible.

First of all, I would like to thank Professor Carlos G. Morales-Guio for his patient teaching and guidance, which has enabled me to work more effectively and learn more efficiently. Also, I would like to thank my lab mate, Kangze Shen, and other members in our group, Joon Baek Jang, Derek Richard, Jun Ke, Maximilian Winzely, as well as the undergraduate students participating in the group meetings. Your assistance, discussions, and suggestions have made working in this lab an incredible warm and wonderful experience.

Secondly, I would like to thank my family and particularly my wife, Bi-Jiun Wang. It has been a rough time for both of us to maintain a long-distance relationship since the beginning of this adventure at UCLA. I really appreciate your unconditional support for my academic pursuit. Without your support, I would not be persistent in this study course. I would also like to thank other members of my family for your encouragements.

Last but not least, I would like to acknowledge support from National Chung-Shan Institute of Science and Technology (NCSIST), Taiwan (R.O.C.) throughout academic years at UCLA. I am really grateful to NCSIST for offering this opportunity of studying abroad. With the support from NCSIST, I was able to initiate this wonderful journey and eventually accomplish it.

There are so many people and things that I could not list and there are too many words to express all the appreciations in my heart. In the end, I am very thankful that UCLA brought me so many unforgettable memories that I will continue to reminisce about.

1. Introduction

1.1 Methane: resources and utilization of natural gas

Methane, not only a major constituent of natural gas, but also known as one of the essential natural energy reserves, has been extensively utilized as raw material or feedstock for production of important base chemicals such as hydrogen, methanol, ammonia, and formaldehyde.[1,2] In addition to abundant resources of natural gas, its utilization offers several competitive advantages globally. From the current energy outlook, natural gas is the prominent option for fuel, energy and feedstock in the chemical and petroleum industries.[3] However, the use of methane is not without issue. Methane in associated petroleum gas cannot be transported economically from remote oil fields and is thus usually flared resulting in significant greenhouse gas (GHG) emissions and energy loss leading to adverse influences on the climate, environment and energy markets. The global chemical and petrochemical subsectors are responsible for over 1.2 gigatons of CO_2 emissions and 150 billion cubic meters of natural gas energy loss every year.[4,5] With increasingly growing concerns of climate change and requirements of environmental conservation, replacing fossil hydrocarbons or converting wasted natural gas into synthetic, sustainable, and environmentally benign chemicals would allow us to reduce GHG emissions, increase resource utilization, and add additional profitability for these oil fields.[6]

Although carbon capture technologies for the chemical manufacturing industry are still in their infancy due to their high capital-intensity and challenges associated with their application at a global scale, the reduction of GHG emissions from the chemical manufacturing sector is still possible through the use of renewable energy as part of the energy mix in manufacturing processes.[7,8] The basic chemical manufacturing industries are the critical link pin between natural gas resources and utilization, and downstream industrial and commercial applications. Instead of

being part of the GHG emission problem, it could become an engine to build significantly decarbonized supply chains from natural resources to commodities and become the creator of a modern, differentiating, intersectoral platform that enclose synergy and flexibility to the production chain through the efficient use of carbon. In this regard, the use of electrocatalytic processes[9] could contribute to the displacement of fossil fuels as heat sources in the energy-intensive chemical transformation processes and deliver more compact, economical, and efficient chemical manufacturing units.

1.2 Current understanding of methane conversion processes

Due to the non-polar and symmetric chemical bonds of methane, it is a highly stable chemical compound with high bond dissociation energy (440 kJ mol^{-1}) that results in difficult C-H bond activation.[2,10] Conventional catalytic processes utilize extreme conditions (high temperatures or pressures) to provide the energy requirements of methane activation and require sophisticated heat integration networks in order to achieve high process efficiency.[2] Primary chemicals derived from methane (Figure 1.1) include syngas, hydrogen, ammonia, methanol, and Fischer–Tropsch liquids. Although methane can be transformed into various chemicals, methane conversion processes for chemicals are still limited in the industrial scale. Currently, methane conversion to chemicals can be classified into two different routes (indirect and direct routes). The indirect route of methane conversion involving a two-step process typically starts from steam methane reforming (SMR) to higher value chemicals via syngas, carbon monoxide and hydrogen, derivatives that represents approximately 96% of current methane oxidation processes for the production of chemicals.[11]

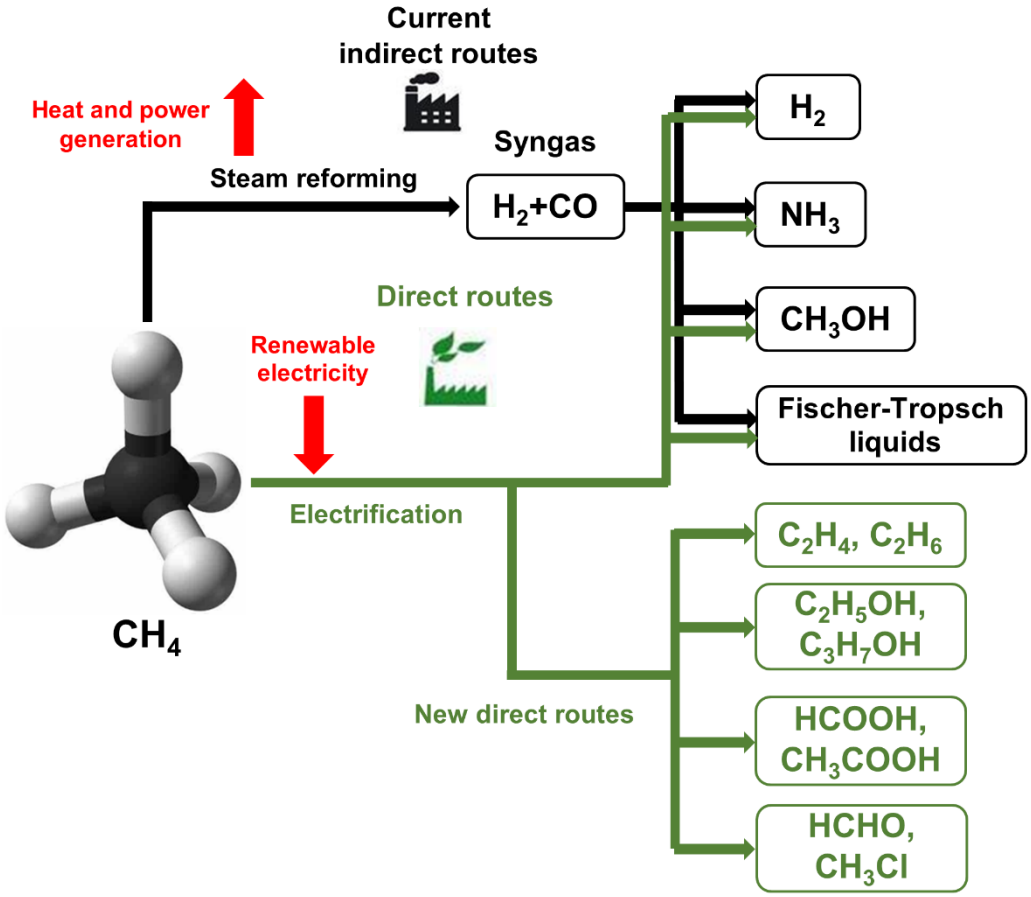

Figure 1.1 Established indirect routes of methane oxidation processes for production of chemicals and potentially alternative or new direct routes via electrification.

SMR is a typical methane oxidation process with highly endothermic reaction to produce chemicals (Equation 1.1) using high temperature (700-1100 °C) and pressure (above 10 bar), where 25-30% of methane feed is burned for necessary heat while the remaining methane is used as feedstock to produce syngas for the subsequent chemical syntheses (Figure 1.1) such as water gas shift (Equation 1.2), ammonia synthesis (Equation 1.3), methanol synthesis (Equation 1.4), and Fischer–Tropsch synthesis.[12]

$$CH_4 + H_2O \rightarrow CO + 3H_2 \qquad \Delta_r H^\circ = 208.7\ kJ\ mol^{-1} \tag{1.1}$$

$$CO + H_2O \rightarrow 3H_2 + CO_2 \qquad \Delta_r H^\circ = -41.1\ kJ\ mol^{-1} \tag{1.2}$$

$$N_2 + 3H_2 \rightarrow 2NH_3 \qquad \Delta_r H^\circ = -91.8\ kJ\ mol^{-1} \tag{1.3}$$

$$CO + 2H_2 \rightarrow CH_3OH \qquad \Delta_r H^\circ = -90.64\ kJ\ mol^{-1} \tag{1.4}$$

$$CH_4 + \tfrac{1}{2}O_2 \rightarrow CH_3OH \qquad \Delta_r H^\circ = -163.5\ kJ\ mol^{-1} \tag{1.5}$$

$$CH_4 + O_2 + e^- + H^+ \rightarrow CH_3OH + H_2O \tag{1.6}$$

From the above synthetic processes, the intermediate syngas can act as a precursor for a variety of chemical synthesis. With the increasing demand to produce these chemicals, the need for the development of advanced technologies for methane activation and transformation continues to grow. The discovery and commercialization of chemical production processes with reduced GHG emissions are of the outmost importance for the chemical industries of the future.

The direct route to produce chemicals,[12] does not require the production of syngas as an intermediate and is primarily based on the formation of either C-O or C-C bonds for methane conversion.[11] For example, methanol is a common C-O bond containing molecule which can be made through the direct conversion of methane with oxygen (Equation 1.5). This methane partial oxidation reaction is usually thermodynamically favorable in the presence of biological, homogeneous, and heterogeneous catalysts.[11,13]

Methane monooxygenase (MMO), a methane-utilizing bacteria, has shown 100% selectivity for methane conversion towards methanol at atmospheric temperature and pressure utilizing oxygen species and electron donors (Equation 1.6).[11,14] Its achievement under ambient conditions has been investigated to direct conversion of methane to methanol derived from the oxygen species at the active sites involved in the biological catalysis. Furthermore, the remarkable selectivity of

methanol implies that MMO can manage the transport of oxygen species, protons and electrons at its catalytic sites for methane oxidation reaction.[13,15,16]

The function of homogeneous catalysis is similar to biological systems that possesses actives sites of both oxygen species and methane in the solvent. Metal complexes (e.g., Fe^{IV}, Cu^{I}, Ru^{III} or Pt^{IV}),[17–20] metal ions with strong affinity of electron acceptor, show high efficiency of methane oxidation to methanol exploiting an oxygen atom insertion into the C-H bond of methane.[11] Here, the methyl radical is the major intermediate under the protection of strong solvent (e.g., trifluoroacetic acid, CF_3COOCH_3) which plays an essential role of not only activating the C-H bond of the active center but also stabilizing the formation of the methyl radical intermediate. The solvent usage contributes to high selectivity and prevents target products from overoxidation.[11,18]

In the field of heterogeneous catalysis, methane partial oxidation processes can be separated into thermal catalysis and electrocatalysis with identical approaches that possess reactivity and morphology similar to biological and homogeneous systems.[2,11–13] Thermal catalysis, utilizing many transition metals in the forms of metals, metal complexes, metal oxides, and metal exchanged zeolites, typically reacts using strong oxidants (N_2O or H_2O_2) or with high thermal energy requirements in order to activate the C-H bond for methane partial oxidation.[2] While electrocatalysis, using molecular oxygen as an oxidant and metal ions with high valences (e.g., Mo, V, Ga, Fe, Co, Mn, and Pd),[11] is capable of tailoring the chemical potential at the catalytic surface and facilitating reactions under atmospheric conditions that renders strong oxidants and high thermal energy requirement unnecessary.[2] Despite electrocatalysis can tune the electrochemical potential for methane partial oxidation, in most of recent reports,[2,10–13,21–25] desirable products usually result in over-oxidizing to carbon dioxide and carbon monoxide which are more thermodynamically favorable. Accordingly, the major challenge is to explore

electrocatalysts that can not only activate the C-H bond of methane but also prevent the desirable products from overoxidation.[11,12]

The other direct methane conversion is the formation of C-C bond to produce higher hydrocarbons (C_2^+ products) including two viable ways: oxidative coupling of methane (OCM) and non-oxidative coupling of methane (non-OCM). OCM is a sophisticated process for methane conversion into hydrocarbons at elevated temperature involving surface catalysis and gas phase coupling reaction corresponding homogeneous and heterogeneous systems simultaneously. With initiating methyl radical through catalyst, gas phase coupling of methyl and allyl radicals will transform methane into ethane or ethylene subsequently (Equation 1.7 and 1.8). In non-OCM, on the other hand, direct methane conversion primarily proceeds via catalyst in the absence of oxygen to form methyl radicals and produce even higher hydrocarbons especially C2 to C7 saturated hydrocarbons (e.g., benzene). [11,26,27]

$$2CH_4 + \frac{1}{2}O_2 \rightarrow C_2H_6 + H_2O \qquad \Delta_r H^\circ = -184.0\ kJ\ mol^{-1} \tag{1.7}$$

$$CH_4 + \frac{1}{2}O_2 \rightarrow \frac{1}{2}C_2H_4 + H_2O \qquad \Delta_r H^\circ = -140.1\ kJ\ mol^{-1} \tag{1.8}$$

Many research efforts have been devoted to direct routes of methane conversion processes economically competitive with indirect routes especially exploiting electrochemical cells.[2,12,13,22] Nonetheless, direct routes of methane conversion to valuable chemicals such as olefins, formaldehydes, and other oxygenates bypassing the transition stage of syngas production have not been well-developed in particularly large-scale industrial processes due to their limited efficiency and low yield or selectivity of desirable products. Still, fundamental studies in electrocatalysis are indispensable and must be integrated within the manufacturing operation units of kinetic protection and selective separation of desirable products.[22] Otherwise, it would be independent of current trends for exploration of flare gas and reduction of GHG emissions.[11] The development of

advanced manufacturing systems and establishment of next generation processes not only maintain the significances of electrochemical cells but also address the challenges of modularity and scalability corresponding to desirable product separation and highly efficient conversion. In these regards, electrochemical cells under harsh and mild conditions will be exceptional of integrating multi-steps into single steps by overcoming the primary limitations of its systems. Although electrochemical systems are still finite because of its stability, durability, modularity, and scalability, the development of these systems is still under way to replace conventional indirect routes of methane conversion.[2,11–13,22,24,25]

1.3 Current state of direct methane oxidation reaction via electrochemical approaches

Research in direct methane oxidation reaction to chemicals via electrochemical approaches has shown significant advances. Most remarkable approach is the development of conductive proton implementing ceramic electrolytes. A $BaZr_{0.8-x-y}Ce_xY_yO_{3-\delta}$ (BZCY) ceramic tube with coating of nickel oxide catalyst is utilized to produce high purity of hydrogen at 91% faradaic efficiency (FE) with nearly whole methane conversion to CO_2 instead of CO. Technoeconomic analysis implies that this design, similar to thermal catalysis system, could be competitive with conventional SMR from the perspective of large scale and a feasible approach to proceed under smaller scale practices. The system utilizing resistive heating and electrochemical separation of protons by the electrolyte internally generate the required heat to counteract the endothermic reaction of SMR.[28] An analogous system is applied in direct ammonia synthesis from methane. The anode part remains the identical SMR reactor while the counterpart applies a Vanadium Nitrate (VN) catalyst, resulting in FE close to 15% and ammonia synthesis rates 1.89×10^{-9} mol s^{-1} cm^{-2} at atmospheric pressure.[29,30]

Methane reforming via electrochemical approaches to produce hydrogen and ammonia has made notable progress while direct methane oxidation to methanol, olefins and other oxygenates has remained challenging due to a trade-off between selectivity and conversion resulting from thermodynamically favorable to CO_x product.[2,10,13,23] Most recently, Vanadium (V)-oxo Dimer clusters in H_2SO_4 have shown methane conversion to CH_3OSO_3H at ambient temperature reaching 84.5% FE under 3 bar methane with decent stability for 240 hours.[31] The reaction in the presence of strong acidic solvent prevents the methanol group from over-oxidizing. Transition metal oxides including NiO/ZrO_2 and Co_3O_4/ZrO_2 have also been explored as alternatives at ambient temperature for electrochemical oxidation of methane in carbonate based electrochemical systems.[24,32] The role of ZrO_2 hypothesizes that non-conductive zirconia participates in the adsorption of carbonate ions to activate methane oxidation under mild conditions. Interestingly, the FEs in some of these systems exceed 100% implying that chemical reactions participate between methane and stoichiometric oxidants in the presence of catalyst or the electrolyte could be responsible for production of oxygenates.

Recent developments have brought electrochemical SMR being economically competitive with conventional SMR. Also, research in direct electrochemical oxidation of methane to methanol, ammonia, and other oxygenates must tackle with the trade-off between selectivity and conversion or be coupled with efficient separation techniques developed to allow production at low conversion but high selectivity.

1.4 Research background, overview, and objectives

1.4.1 Research background

Electrochemistry, a powerful technique, utilizes the chemical potential of redox reactions to provide an economical alternative for direct electrochemical methane oxidation into target chemicals. Electrochemical processes have shown extraordinary advantages such as relatively low cost with cost-effective electric power, typically proceeding under ambient conditions of temperature and pressure, feasible modularity and scalability, and is also seen as an example of green chemistry when coupled to renewable sources of electricity. More importantly, in electrochemical processes, either the oxygen site on the electrode surface or free radicals generated at the electrode/electrolyte interface can activate methane.[2,12,22] Not only can operating conditions be tailored to enhance kinetics and the rate of methane conversion, but their selectivity can be tuned through applied potentials. Recent research and development of electrochemical oxidation of methane to methanol under atmospheric conditions has been a topic of significant interest to address the high energy requirement in conventional thermal catalysis and provide alternatives to wasted flaring. Typically, electrochemical oxidation of methane is more favorable at relatively low overpotentials (Equation 1.9) while it is kinetically sluggish and may require higher overpotential to drive the rate-limiting step. However, the oxygen evolution reaction (OER, Equation 1.10) usually occurs at high overpotentials and competes with methane oxidation, resulting in reduced methane activation. From this perspective, electrochemical processes in methane oxidation have been undertaken to investigate the desirable products, particularly methanol and potentially other oxygenates or higher hydrocarbons.[10,13,23,25]

$$CH_{4(g)} + H_2O_{(l)} \rightarrow CH_3OH_{(l)} + 2H^+ + 2e^- \qquad E^\circ = 0.58\ V\ vs\ SHE \tag{1.9}$$

$$H_2O_{(l)} \rightarrow O_{2(g)} + 4H^+ + 4e^- \qquad E^\circ = 1.23\ V\ vs\ SHE \tag{1.10}$$

1.4.2 Research overview

Many works in the literature have demonstrated transition metal oxides as alternative methane oxidation catalysts via electrochemical processes. Mustain and co-workers have shown binary transition metal oxides of NiO/ZrO_2 in carbonate electrolyte to catalyze the electrochemical oxidation of methane.[24,33] An analogous example was published by Ma et al. utilizing chemical precipitation of Co_3O_4/ZrO_2 nanocomposite and Co_3O_4 powder/ZrO_2 nanotubes to produce higher alcohols such as 1-propanol and 2-propanol.[32,34] Introducing zirconia by using co-precipitation to unary transition metal oxide as catalyst has shown to promote the methane oxidation in the presence of carbonate ions enabling the system to operate at room temperature.[24,32–34] Aditya et al. have demonstrated a comprehensive work on 12 different transition metal oxides (TMOs) utilizing transient open circuit potential (t-OCP) to determine the stable active sites of TMOs. There are 4 TMOs (TiO_2, IrO_2, PbO_2, and PtO_2) being reported that are active for methane oxidation reaction towards methanol. Furthermore, two reaction pathways of intermediates have been proposed: CH_x intermediate at lower potentials while $^*CH_xO_y$ intermediate at higher potentials. In addition to unary TMOs, they developed a bimetallic Cu_2O_3 on TiO_2 catalyst, where Cu overcomes the reaction barrier for the key intermediates of $^*CH_3$ and $^*OH$ and facilitates the desorption of $^*CH_3OH$, and FE is up to 6%. It implies that using bimetallic TMOs provides an alternative way to advance electrochemical oxidation of methane.[35]

Recent reports of electrocatalysts and electrolytes for the oxidation of methane to higher value chemicals via electrochemical approaches are compiled in terms of operating conditions, products, and faradaic efficiencies in Table 1.1.[24,31–34,36–40] Despite the electrochemical oxidation of methane to various chemicals being demonstrated in many reports, results are inconsistent due to the use of various conditions of catalysts and electrolytes. This highlights the difficulties to

determine product distribution accurately for methane partial oxidation and result in a lack of fundamental understandings of the kinetics associated with these electrochemical systems. It is crucial that the discussion of reaction mechanisms, computational chemistry, and optimization of reaction environments is built upon reliable experimental evidence. In this work, we demonstrate that most of the work in the existing literature is unreliable as it is affected by the electrochemical conditions on which it is collected. Importantly, this thesis work is the first attempt towards a systematic understanding of methane electrochemistry.

Table 1.1. Summary of current state-of-the-art literatures for electrochemical oxidation of methane to valuable chemicals

Electrocatalysts	Temp. (°C)	Pressure (bar)	Oxidant source	Electrolyte	Technique/ Method	Products	Methane conversion (%)	Selectivity (%)	Faradaic efficiency (%)	Ref.
Pt	130	46.5	$(V^{IV}O)(SO_4)$	$K_2Pt^{II}Cl_4$ with NaCl	Three-electrode cell	CH_3OH, CH_3Cl, $CH_2(OH)_2$, HCOOH	13-16	CH_3OH: 70	90-103	[36]
NiO/ZrO_2	40	1	O_2	Na_2CO_3	Membrane electrode assembly	CH_3OH, HCHO, HCOOH, C_2H_5OH, CH_3COOH, C_3H_8O, C_3H_6O		HCHO: 44	(> 100)	[24]
nanotube ZrO_2/Co_3O_4	25	1	CO_3^{2-}	Na_2CO_3	Three-electrode cell	C_2H_5OH, $CH_3CH_2CH_2OH$, $CH_3CH(OH)CH_3$		91.98 ($CH_3CH_2CH_2OH$, and $CH_3CH(OH)CH_3$)	(> 100)	[34]
ZrO_2/Co_3O_4	25	1	CO_3^{2-}	Na_2CO_3	Three-electrode cell	$CH_3CH_2CH_2OH$, $(CH_3)_2CHOH$, CH_3CHO,	40	>60 (total)	(> 100)	[32]
$ZrO_2/NiCo_2O_4$	25	1	CO_3^{2-}	Na_2CO_3	Three-electrode cell	$CH_3CH_2CH_2OH$, $CH_3CH(OH)CH_3$, CH_3CH_2COOH, CH_3COCH_3,	47.5	CH_3CH_2COOH: 65	100	[37]
(V)-oxo dimer	25	3	SO_4^{2-}	H_2SO_4	Three-electrode cell	CH_3OSO_3H	100	100	F.E.= 85-90	[31]
NiO/Ni	25	1	OH^-	NaOH	Two-electrode cell	CH_3OH, C_2H_5OH	100	87	F.E.= 89	[38]
NiO/Ni hollow fiber	25	1	OH^-	NaOH	Three-electrode cell	CH_3OH, C_2H_5OH		CH_3OH: 78 C_2H_5OH: 95	CH_3OH F.E.= 54 C_2H_5OH F.E. = 85	[39]
$TiO_2/RuO_2/V_2O_5$	25	1	H_2O	Na_2SO_4	Three-electrode cell	CH_3OH, HCHO, HCOOH	100	CH_3OH: 97.7	57	[40]
NiO/ZrO_2	25	1	O_2	Na_2CO_3	Membrane electrode assembly	CH_3OH			F.E. = 5	[33]

1.4.3 Research objectives

In this thesis work, an electrodeposition method will be utilized to synthesize unary (CoO_x, NiO_x, MnO_x, FeO_x, and CuO_x) and binary ($CoZrO_x$) transition metal oxides[41] (Figure 1.2) that will be used as electrocatalysts for the oxidation of methane. The intrinsic properties of transition metal oxides such as catalyst composition, oxidation state, the nature of active sites, and the concentration of reactant within the boundary layer during electrocatalysis will be studied for methane partial oxidation and will be compared with other catalyst preparations from the literature. More importantly, a systematic study of various experimental conditions (i.e. applied potential, current, temperature, pressure, pH, and boundary layer thickness) and their effects on determining methane activation rates and product selectivity will be presented. The work presented here should allow us to construct a better understanding of how various parameters affect the kinetics for product formation and thus contribute to the development of this field.

This study aims to provide a qualitative elucidation of the electrochemical oxidation of methane to methanol process for electrocatalyst exploration that could meet theoretical simulation used to rationalize the experimental observations. The combination of theory and experiments (Figure 1.3) may enhance the fundamental understandings of electrocatalyst activity, electrolyte engineering, mass transfer limitation, and methanol production. The preliminary results of proposed study will be applicable to the electrocatalyst development for direct routes of methane to methanol and may also explore other chemicals such as oxygenates and higher hydrocarbons.

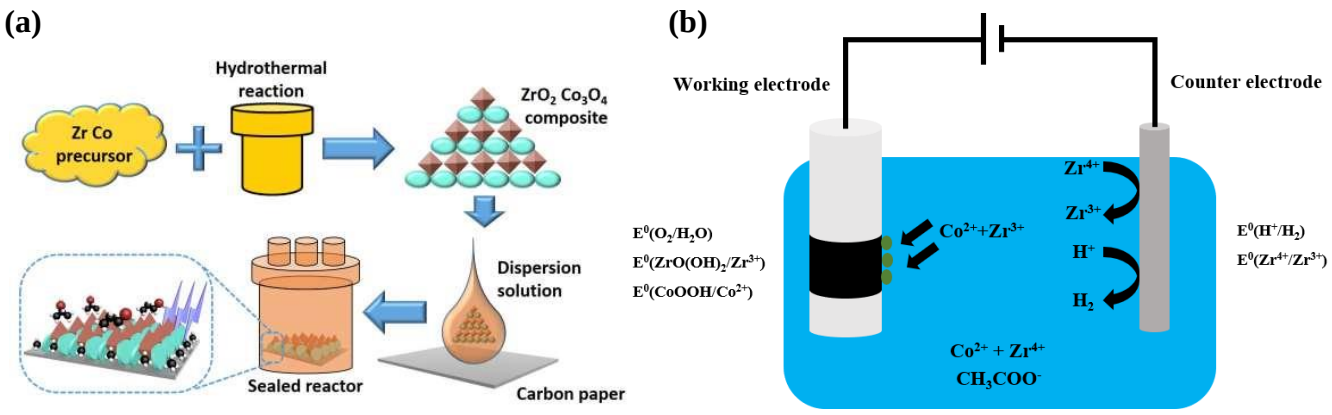

Figure 1.2. Schematics of electrocatalyst synthesis for Co_3O_4/ZrO_2 (a) chemical co-precipitation preparation. It has been mostly utilized to prepare electrocatalysts involving multiple steps such as centrifugation, collection, drying, and annealing. The schematic of electrocatalyst synthesis has been adapted from [32]. (b) electrical co-deposition synthesis. It only requires one step utilizing potential driven approach to form binary electrocatalysts.

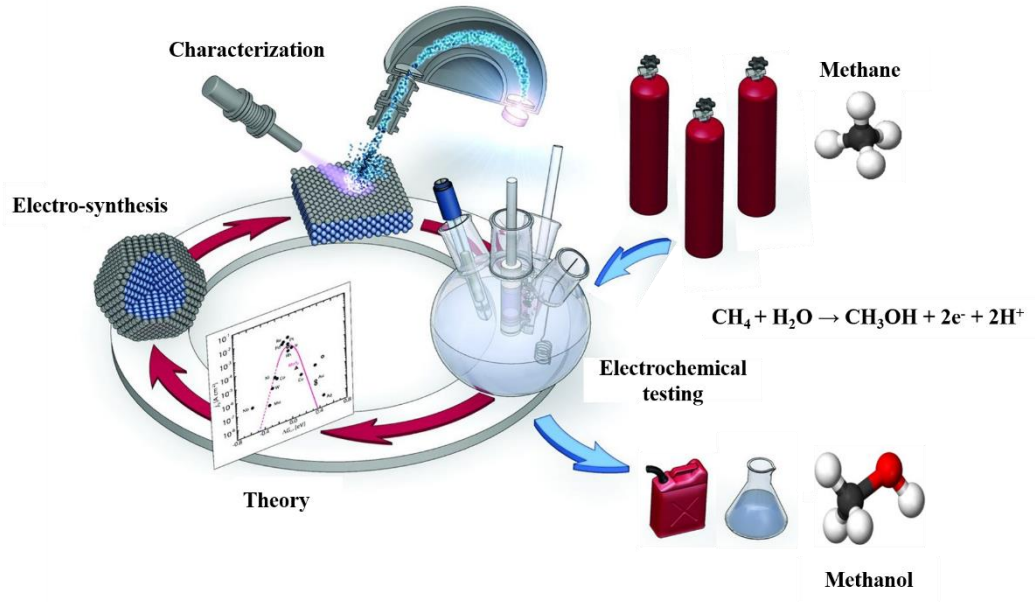

Figure 1.3. Study approach combining theory and experiment to enhance fundamental understandings of electrochemical partial oxidation of methane towards methanol.

2. Experimental section

2.1 Electrocatalyst materials and preparation

Sodium acetate (NaOAc, anhydrous, ≥99%), Cobalt(II) chloride ($CoCl_2$, anhydrous, >98%), zirconium(IV) acetate hydroxide($(CH_3CO_2)_xZr(OH)_y$), and manganese(II) chloride ($MnCl_2$, tetrahydrate, 97%) were purchased from Sigma-Aldrich. Nickel(II) acetate (NiOAc, tetrahydrate, 98%), iron(II) chloride ($FeCl_2$, tetrahydrate, 99%), and copper(II) acetate ($Cu(CH_3COO)_2$, anhydrous, 99%) were purchased from Fisher Scientific. Millipore deionized water (18.2 MΩ cm) was used to prepare all of the electrodeposition baths. The concentrations of precursors used in electrodepositions of the different catalysts and specific pH are compiled in Table 2.1. Sodium acetate (0.1 M NaOAc) was used in all of the electrodeposition baths as supporting electrolyte. The pH of the baths was adjusted using either 0.1 M acetic acid solution or 0.1 M sodium hydroxide solution. All of the electrodeposition experiments were carried out under atmospheric conditions unless mentioned otherwise.

Table 2.1. Concentrations and pH of precursors in the electrodeposition baths

Catalyst	$CoCl_2$	$(CH_3CO_2)_xZr(OH)_y$	NiOAc	$MnCl_2$	$FeCl_2$	$Cu(CH_3COO)_2$	pH
$CoZrO_x$	16 mM	5 mM	--	--	--	--	5.5-6
CoO_x	16 mM	--	--	--	--	--	5.5-6
NiO_x	--	--	16 mM	--	--	--	7.5-8
MnO_x	--	--	--	16 mM	--	--	5.5-6
FeO_x	--	--	--	--	16mM	--	7.0-7.5
CuO_x	--	--	--	--	--	16 mM	5.5-6

2.2 Catalyst electrodeposition

An autolab PGSTAT302N potentiostat/galvanostat was used for electrodeposition in a three-electrode setup with a titanium cylinder substrate (area = 3 cm^2) as the working electrode, a graphite foil as the counter electrode, and an Ag/AgCl sat. KCl as the reference electrode. Prior to use, the surface of titanium cylinder electrode was polished by using an alumina slurry suspension of 0.05 mm grain size on a microcloth polishing pad (Buehler), rinsed thoroughly with Millipore deionized water (18.2 MΩ cm), and sonicated in deionized water for 10-15 minutes. Prior to electrodeposition, the titanium cylinder electrode was immersed in the solution of 2.5 M hydrochloric acid for 30−60 minutes to remove surface oxides. The Ti cylinders were then rinsed in deionized water and dried under Ar flow. In the electrodeposition process, all of the applied potentials were measured against the Ag/AgCl sat. KCl reference electrode. Except copper, electrodeposition of most catalysts was performed by 100 cycles of consecutive linear sweeps within a specific potential window from 0.8 to 1.1 V vs Ag/AgCl at 10 mV s^{-1}. The current efficiency during the oxidative deposition is the fraction of electrons collected by the working electrode that are involved in the deposition of the catalyst. The deposition of most metal (oxy)hydroxides (e.g., $M^{2+}(aq) \rightarrow MOOH(s) + e^- + 3H^+$) was done using oxidative potentials while copper was obtained by applying constant potential (−0.18 V vs Ag/AgCl) for 5 min via reductive deposition of the catalyst ($2Cu^{2+} + 2e^- + H_2O \rightarrow Cu_2O + 2H^+$).

2.3 Electrochemical measurements

All the parts and accessories were purchased from PINE research. The titanium cylinder electrode (diameter: 12 mm) used in this work was inserted in a rotating cylinder electrode (RCE) tip by assembling main body, PTFE seal washer, PTFE compression washer, and PCTFE keeper nut and then connected to the shaft. Prior to electrochemical setup, the electrodeposited titanium cylinder electrode was rinsed thoroughly with deionized water. A three-electrode glass cell setup was used with the titanium cylinder as the working electrode, the platinum wire with a fritted glass tube as the counter electrode, the Ag/AgCl sat. KCl as the reference electrode, and the solution of 0.1 M potassium carbonate (K_2CO_3) as the electrolyte. Prior to electrochemical measurements, high purity of argon gas (Ar, 99.999%) as the inert gas or methane gas (CH_4, 99.999%) as the reactant were used in the experiments. Before experiments, the electrolyte was bubbled for 30 minutes with Ar or CH_4 to prepare the saturated environment.

In the electrochemical measurements, the uncompensated resistance was determined by using electrochemical impedance spectroscopy (EIS) from the response at the high-frequency (f > 100 kHz) for measuring and correcting potential drop across the resistance of the solution. The activities of various catalysts were determined by cyclic voltammetry. The long-term electrochemical oxidation of methane was conducted in the three-electrode cell setup with a closed system by using chronoamperometry and multiple samples were taken to detect liquid products that specific time of sampling was discussed and shown in the following results and discussion section. All the electrochemical measurements were automated by using the Autolab PGSTAT302N potentiostat/galvanostat and the application of the Nova V2.1 software connected a PINE AFMSRCE rotator as is shown in Figure 2.1.

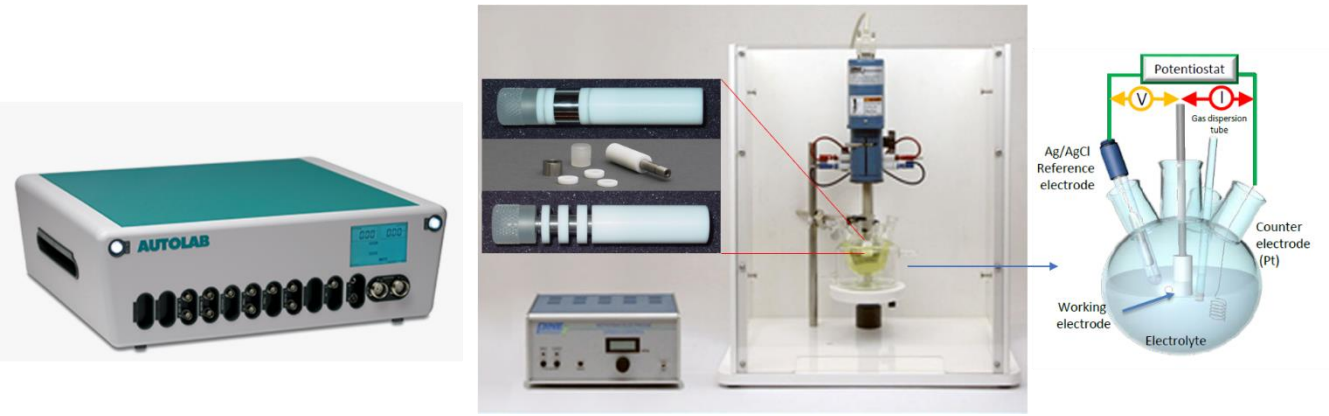

Figure 2.1. Electrochemical measurement setup including electrochemical cell (right); rotator, shaft, and workstation (middle); and potentiostat (left).

2.4 Characterization and product analyses

Morphology and microstructure analyses of the samples were carried out using scanning electron microscopy (SEM, JEOL JSM 6700 F). Kratos X-ray photoelectron spectroscopy (XPS) was used to determine element composition of different catalyst covering its surface as well as their oxidation state. The detection of liquid products was analyzed after electrolysis using 500 MHz nuclear magnetic resonance (DRX500 spectrometer Bruker Biospin GmbH), where the samples were prepared by mixing 700 µL of the product solution with 35 µL internal standard comprising of D_2O, DMSO, and phenol.

3. Mathematical modeling

3.1 Model of electrocatalysts on methane partial oxidation:

To estimate changes in the local pH of the electrolyte/electrode interface during experiments, a mathematical model was developed. The conservation equation is introduced combined with the experimental data collected to calculate the local pH, the concentration of bicarbonate ions and carbonate ions, and the concentration of CO_2 on the surface of electrode.

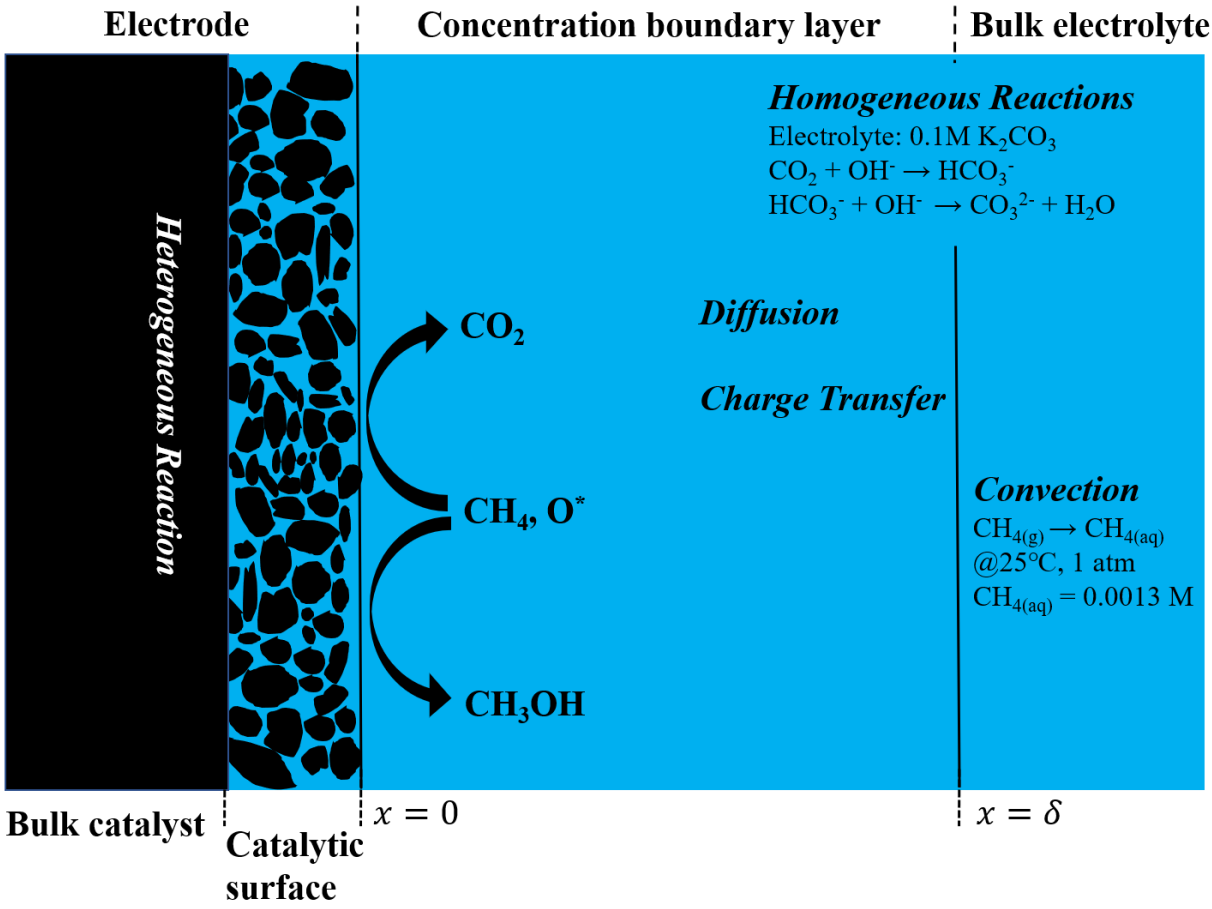

Figure 3.1. One dimensional schematic of the concentration boundary layer. The reactions occur within the boundary layer that has been highlighted in terms of mass transport effects. The position, x axis, in this work is defined as the distance away from the catalytic surface.

Figure 3.1 shows the electrolyte/electrode interface boundary layer in the system for electrochemical oxidation of methane. In a typical experiment, 0.1 M K_2CO_3 is used as the electrolyte and is saturated by bubbling methane in the bulk of the electrolyte. The model assumes that all the CO_2 generated through the overoxidation of methane would be absorbed by the bulk electrolyte. Heterogeneous reactions involve water oxidation (Equation 3.1) and methane oxidation towards methanol (Equation 3.2) and carbon dioxide (Equation 3.3). Homogeneous reactions in bulk electrolyte are also listed below (Equation 3.4 and 3.5).

$$2H_2O \rightarrow 4e^- + 4H^+ + O_2 \tag{3.1}$$

$$CH_4 + O^* \rightarrow CH_3OH \tag{3.2}$$

$$CH_4 + 4O^* \rightarrow CO_2 + 2H_2O \tag{3.3}$$

$$CO_2 + OH^- \leftrightarrow HCO_3^- \qquad K = 3.3 \times 10^7 \tag{3.4}$$

$$HCO_3^- + OH^- \leftrightarrow CO_3^{2-} + H_2O \qquad K = 4.7 \times 10^3 \tag{3.5}$$

The rate constants for the forward and reverse reactions (3.4 and 3.5) are given in Table 3.1. The dissociation constant of water (K_w), and the dissociation constants of carbonic acid (K_{a1}) and bicarbonate buffer (K_{a2}) are given in Table 3.2. The diffusion coefficients are collected in Table 3.3 using Stokes– Einstein's equation ($D\mu/T$ = constant at T = 298 K) for different species in water at 25 ℃.

Table 3.1. Rate constants for reactions (3.4) and (3.5) at 25 ℃.

Reaction	Forward rate constant (M^{-1} s^{-1})	Reverse rate constant (s^{-1})
(3.4)	$k_{1f} = 7.7\times10^3$	$k_{1r} = 2.3\times10^{-4}$
(3.5)	$k_{2f} = 1\times10^8$	$k_{2r} = 2.15\times10^4$

Table 3.2. Dissociation constants for water, carbonic acid, and bicarbonate buffer.

K_w	K_{a1}	K_{a2}
1×10^{14}	4.5×10^{-7}	4.7×10^{-11}

Table 3.3. Diffusion coefficients for different species in water at 25 °C (Unit: $cm^2\ s^{-1}$).

D_{H^+}	D_{OH^-}	D_{CH_4}	D_{CO_2}	$D_{HCO_3^-}$	$D_{CO_3^{2-}}$
9.3×10^{-5}	5.27×10^{-5}	1.84×10^{-5}	1.91×10^{-5}	9.23×10^{-6}	1.19×10^{-5}

Film theory is assumed to be applicable and followed by Nernst-Planck equation where, in the concentration boundary layer, the velocity gradients or convective effects are negligible and the conservation equation can be written for all species in the simplified form below:

$$\frac{\partial C_i}{\partial t} = \frac{\partial}{\partial x}\left(D_i \frac{\partial C_i}{\partial x}\right) + R_i$$

The following conservation equations including the reaction rate terms for equation (3.4) and (3.5) for all species can be written as the following terms (Equations 3.6–3.11):

$$\frac{\partial [H^+]}{\partial t} = D_{H^+} \frac{\partial^2 [H^+]}{\partial x_2} \tag{3.6}$$

$$\frac{\partial [OH^-]}{\partial t} = D_{OH^-} \frac{\partial^2 [OH^-]}{\partial x_2} - k_{1f}[CO_2][OH^-] + k_{1r}[HCO_3^-] - k_{2f}[HCO_3^-][OH^-] + k_{2r}[CO_3^{2-}] \tag{3.7}$$

$$\frac{\partial [CH_4]}{\partial t} = D_{CH_4} \frac{\partial^2 [CH_4]}{\partial x_2} \tag{3.8}$$

$$\frac{\partial [CO_2]}{\partial t} = D_{CO_2} \frac{\partial^2 [CO_2]}{\partial x_2} - k_{1f}[CO_2][OH^-] + k_{1r}[HCO_3^-] \tag{3.9}$$

$$\frac{\partial[HCO_3^-]}{\partial t} = D_{HCO_3^-}\frac{\partial^2[HCO_3^-]}{\partial x_2} + k_{1f}[CO_2][OH^-] - k_{1r}[HCO_3^-] - k_{2f}[HCO_3^-][OH^-] + k_{2r}[CO_3^{2-}] \quad (3.10)$$

$$\frac{\partial[CO_3^{2-}]}{\partial t} = D_{CO_3^{2-}}\frac{\partial^2[CO_3^{2-}]}{\partial x_2} + k_{2f}[HCO_3^-][OH^-] - k_{2r}[CO_3^{2-}] \quad (3.11)$$

The conservation equations (3.6–3.11) are second order time dependent partial differential equations that have to be solved under the following boundary conditions. First of all, the initial values of concentrations for different species (t = 0, before reaction occurs) are listed in Table 3.4.

Table 3.4. Initial equilibrium values (at t = 0) for H^+, OH^-, CH_4, H_2CO_3, HCO^{3-} , and CO_3^{2-} and pH at 0.1 M potassium carbonate electrolyte (K_2CO_3) at 25 ℃.

Electrolyte concentration (M)	H^+ (M)	OH^- (M)	CH_4 (M)	H_2CO_3 (M)	HCO_3^- (M)	CO_3^{2-} (M)	pH	Viscosity ($cm^2\ s^{-1}$)
0.1	1.9953×10^{-12}	5×10^{-3}	1.3×10^{-3}	1.8×10^{-8}	4.1×10^{-3}	9.6×10^{-2}	11.70	1.015×10^{-2}

Secondly, at time t > 0 and x = 0 (the interface between bulk solution and the boundary layer), the experiment is conducted under 800 rpm at ambient temperature and pressure,

$$-OH^-_{comsumpion} = D_{OH^-}\frac{\partial[OH^-]}{\partial x} = j_{total}/F \quad (3.12)$$

$$-CH_{4\ consumption} = D_{CH_4}\frac{\partial[CH_4]}{\partial x} \quad (3.13)$$

$$CO_{2\ formation} = D_{CO_2}\frac{\partial[CO_2]}{\partial x} \quad (3.14)$$

where the [OH^-], [CH_4], and [CO_2] are the concentration occurring at the interface. The average current conducting in the experiments is 3×10^{-5} (A) presenting on the active surface area 3 cm^2 of the electrode and the methanol production is approximately 3×10^{-5} (M) for 20 minutes reaction time in the 0.1 L carbonate electrolyte. Therefore, the methane consumption and carbon dioxide formation are 3.71×10^{-6} and 2.78×10^{-6} (mmol cm^{-2} s^{-1}), respectively.

Lastly, the boundary conditions at time $t > 0$ and $x = \delta$ (the boundary layer of bulk solution) are the same equilibrium values in the bulk solution (The boundary layer thickness is assumed to be 3×10^{-3} cm).

$$[H^+] = [H^+]_{bulk} \tag{3.15}$$

$$[OH^-] = [OH^-]_{bulk} \tag{3.16}$$

$$[CH_4] = [CH_4]_{bulk} \tag{3.17}$$

$$[CO_2] = 0 \tag{3.18}$$

$$[HCO_3^-] = [HCO_3^-]_{bulk} \tag{3.19}$$

$$[CO_3^{2-}] = [CO_3^{2-}]_{bulk} \tag{3.20}$$

With all the conservation equations (3.6) – (3.11), the boundary conditions (3.12) – (3.20), and constants known, the partial differential equations given can be solved using the function 'pdepe' in MATLAB. Variations in the concentration of different species and local pH as a function of distance and time for the electrocatalyst CoO_x electrodeposited on the titanium electrode for the electrochemical oxidation of methane are shown in Figure 3.2.

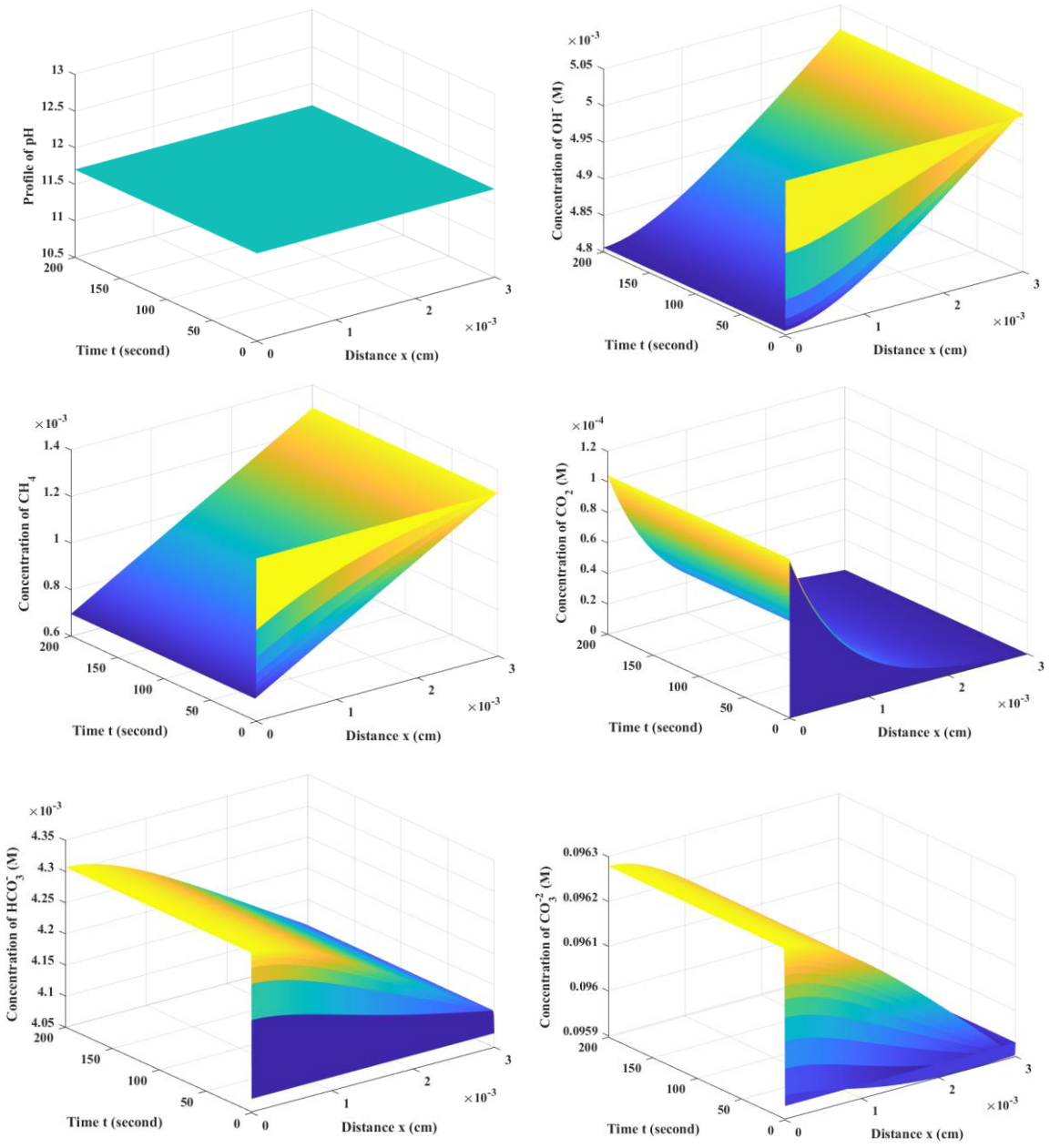

Figure 3.2. Concentration profiles of all different species and local pH involved when using an electrodeposited CoO_x onto titanium cylinder electrode with electrolyte of 0.1 M K_2CO_3 for the electrochemical oxidation of methane.

3.2 Partial current density of methane oxidation towards methanol

The experiment is conducted under 800 rpm at ambient temperature and pressure using an electrodeposited catalyst onto titanium cylinder electrode with 0.1 M K_2CO_3 electrolyte for the electrochemical oxidation of methane. The values of partial current density (PCD) regarding methane oxidation towards methanol calculating the theoretical maximum and methane flux that may determine whether the experimental results could be rationalized. The maximum PCD can be calculated by the limiting current flow for the electrochemical reaction (Equation 3.21),

$$i_{CH_4,limiting} = zFC_{CH_4}K_mA \tag{3.21}$$

where z is the stoichiometric number of electrons consumed in the electrochemical reaction (2 for methane oxidation to methanol), F is Faraday's constant 96,485 (C mol^{-1}), C_{CH_4} is the initial concentration saturated in the bulk electrolyte 1.3×10^{-3} (M), K_m is the mass transfer coefficient 8.2×10^{-3} (cm s^{-1}) adapted from Pine research: Study of Mass Transport Limited Corrosion with Rotating Cylinder Electrodes [42] (Equation 3.22), and A is the active surface area 3 cm^2,

$$K_m = 0.01d^{0.4}\left(\frac{\mu}{\rho}\right)^{-0.344}D^{0.644}F^{0.7} \tag{3.22}$$

where d is the diameter of rotating cylinder electrode 1.2 (cm), μ is the viscosity 1.015×10^{-2} (cm^2 s^{-1}), ρ is the density 1 (g cm^{-3}), and D is the diffusion coefficient 1.84×10^{-5} (cm^2 s^{-1}), and F is the rotational speed 800 (rpm). Considering all the methane species reacted by the electrochemical reaction, the limiting current (maximum PCD) for methanol production is 6.17 (mA) and the methane flux is 7.973×10^{-9} (mol cm^{-2} s^{-1}) from Fick's law with the previous assumption of 30 μm boundary layer thickness. Consequently, the expected maximum methanol concentrations in the 0.1L carbonate electrolyte are 1.15 mM and 2.3 mM for one-hour and two-hours experiments, respectively.

4. Results and discussion

4.1 Electrodeposition of transition metal oxides

An electrodeposition method was employed to fabricate binary ($CoZrO_x$) and unary (CoO_x, CuO_x, NiO_x, FeO_x, and MnO_x) transition metal oxides (For details, see the Experimental Section 2.1 and 2.2). As shown in Figure 4.1, scanning electron microscopy (SEM) was used to observe the morphology and microstructure of different transition metal oxides. In all samples, different transition metal oxides were analyzed before and after electrochemical oxidation of methane for comparisons. The binary transition metal oxide of $CoZrO_x$ was successfully synthesized via zirconium co-electrodeposition with cobalt oxide onto the surface of titanium cylinder electrode, with the zirconium crystal particle attached to the crystalline cobalt oxide (Figure C.1).

In Figure 4.1. (a), the SEM image of blank titanium showed a flat surface without any fine structure for comparisons. Cobalt oxide is electrodeposited as a dense film before the electrochemical oxidation of methane (Figure 4.1 (b)). By contrast, cobalt oxide after oxidation formed loose lump patterns which implies that some catalytic oxides were lost during testing. In Figure 4.1. (c), Copper oxide before oxidation showed angular particles with edges and corners closely packed onto the substrate with a dense orientation. Conversely, copper oxide after oxidation showed smoother crystals and a less dense orientation. In Figure 4.1. (d), Nickel oxide before oxidation exhibited a sheet morphology and relatively flat microstructure showing plates on the substrate. Some of the sheets stacked together into a larger plane while others extruded with each other to form cracks and smaller sheets. In contrast, nickel oxide after oxidation demonstrated crack textures on its plane.

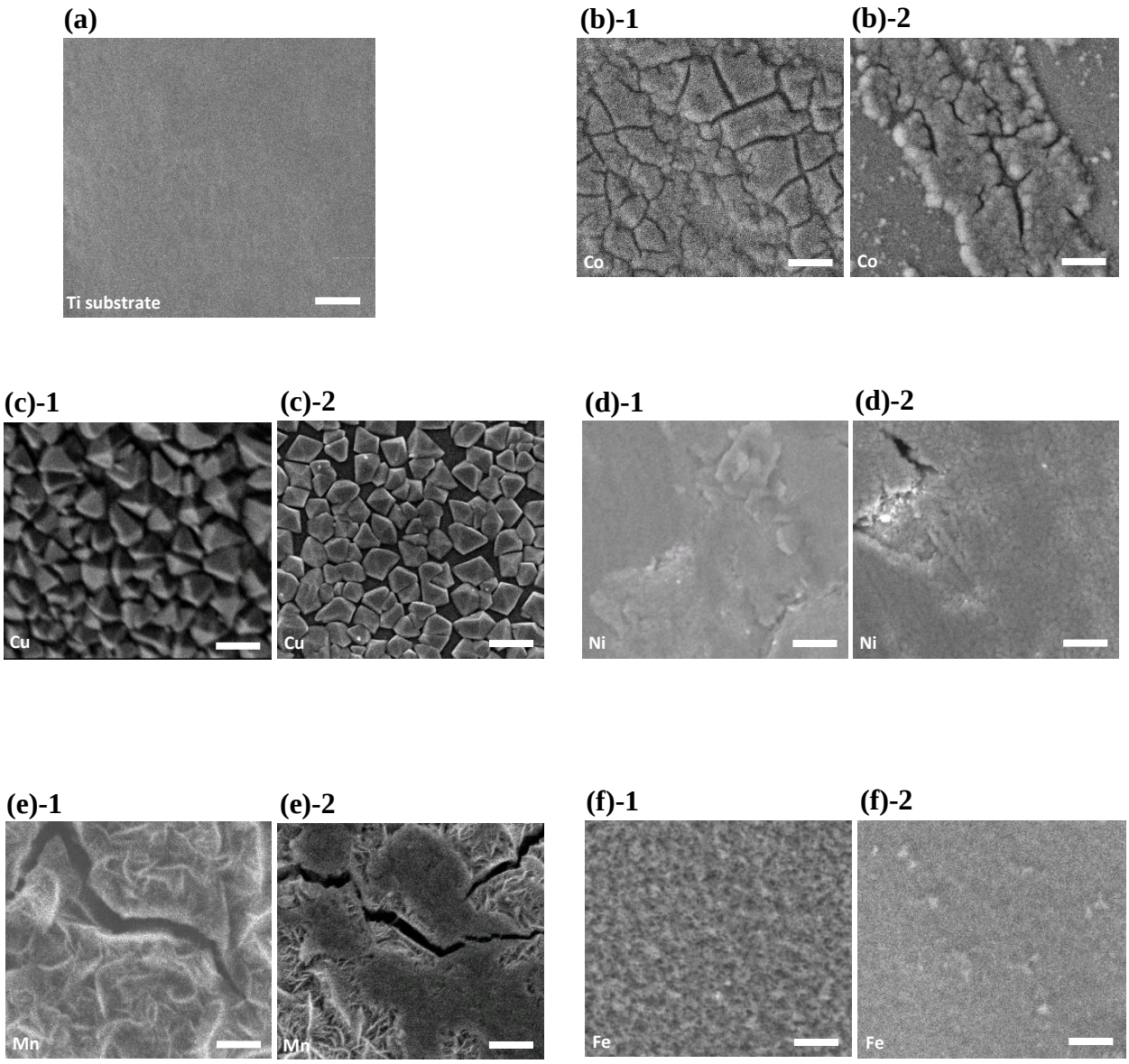

Figure 4.1. SEM images of (a) blank titanium and different transition metal oxides (b) CoO_x (c) CuO_x (d) NiO_x (e) MnO_x and (f) FeO_x electrodeposited on titanium cylinder electrode. 1 denotes samples before electrochemical oxidation of methane. 2 denotes samples after electrochemical oxidation of methane. The scale bars in all the samples are 1 μm.

In Figure 4.1. (e), manganese oxide presented larger fragments and small sheets packed on the surface when electrodeposited onto substrate, where its stacked oxide and lattice orientation showed poor substrate adhesion. Manganese oxide after oxidation, on the other hand, resulted in some of the small sheets being lost to give a flat surface while the larger fragments remained on the surface. Iron oxide before oxidation showed a porous structure packed with small particles exhibiting dense orientation (Figure 4.1. (d)), while its porous microstructure could not be obviously seen after oxidation and only a few porous sites remained where the flat substrate indicated that iron oxide was lost. In the view of these figures, SEM images of all the different transition metal oxides ($CoZrO_x$, CoO_x, CuO_x, NiO_x, MnO_x, and FeO_x) have been shown before and after electrochemical oxidation of methane in order to give a general idea of morphology and microstructure of different electrocatalysts electrodeposited and presented on the substrate for further studies.

Additionally, the chemical compositions and oxidative valences (oxidation states) of binary transition metal oxide ($CoZrO_x$) was measured by X-ray photoelectron spectroscopy (XPS). Figure C.2. showed wide-range, Co 2p, Zr 3p, and O 1s XPS spectra for binary transition metal oxide $CoZrO_x$. It indicates that binary transition metal oxide most likely consisting of a mixture of ZrO_x and CoO_x was successfully co-electrodeposited on the titanium cylinder electrode. Furthermore, the intensity of the Ti 2p in the XPS spectra is low compared to Co 2p and Zr 3p and implies that the surface of titanium cylinder electrode is well covered through electrodeposition and all the active materials are presented on the surface for electrochemical oxidation of methane. The Co:Zr ratio in the $CoZrO_x$ film is approximately 1:4 according to XPS spectra. *Ex situ* XPS showed a Co 2p signal in $CoZrO_x$ that correspomds to Co^{2+} with the main Co $2p_{3/2}$ signal of binding energy (BE) 780.3 eV. Zirconium, on the other hand, is an oxidative state of Zr^{4+} with the primary

Zr $3d_{5/2}$ signal of BE 182.2 eV. The signal in the O 1s region at BE = 531.4 eV corresponds to oxygen atoms similar to the formation of transition metal oxides. It was hypothesized that the incorporated zirconia into CoO_x occurred through an electrodeposition mechanism involving the reduction of Zr^{4+} to Zr^{3+} on the counter electrode and subsequent oxidative deposition of $Zr^{3+}$and Co^{2+} on the working electrode.

The chemical compositions of titanium substrate and unary transition metal oxides (CoO_x, CuO_x, NiO_x, MnO_x, and FeO_x) were also measured by wide-range XPS spectra (Figure 4.2) and the elemental distributions are listed in Table 4.1. The titanium substrate showed typical signals of Ti 2p and O 1s. The other unary transition metal oxides also showed typical signals of their main elements (Co 2p, Cu 2p, Ni 2p, Mn 2p, and Fe 2p) and O 1s which indicated that the oxygen atoms correspond to the formation of transition metal oxides. A few electrocatalysts (CoO_x, CuO_x, and NiO_x) contain a little amount of Ti 2p signals which implies that the surfaces of titanium cylinder electrode were not fully covered through electrodeposition while MnO_x, and FeO_x were fully covered on the titanium substrate with larger mass loadings. Additionally, the mass loadings of MnO_x is responsible for the observed potassium ions in the C 1s region after the electrochemical oxidation of methane since the layered oxides containing different valences of metal oxides confine anions and water between its interlayers for the charge of the metal oxide layers. The trace amount of the Cl 2p signals in some of the XPS spectra could be the acid cleaning of HCl solution prior to the electrodeposition in order to remove the titanium oxides.

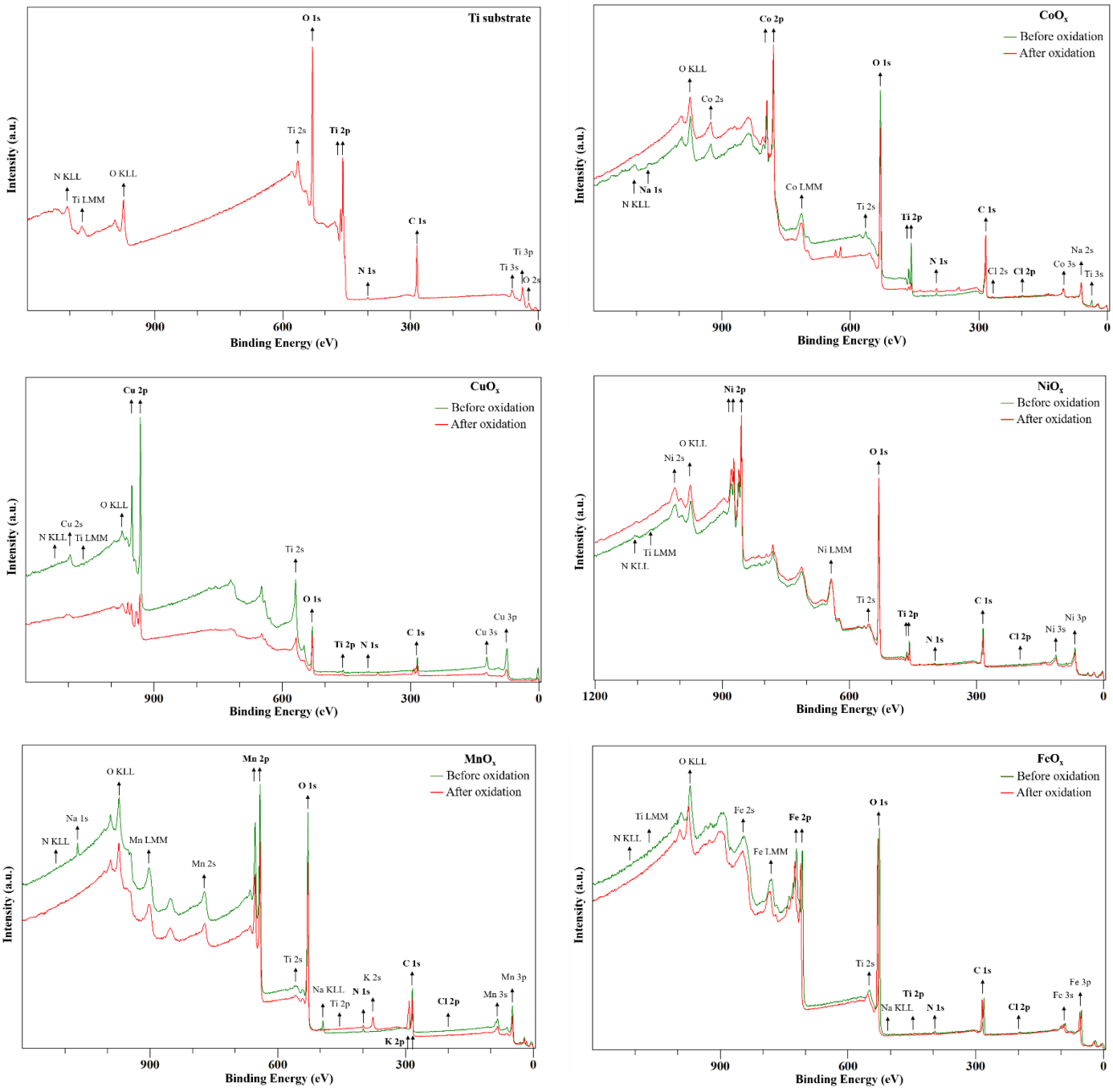

Figure 4.2. Wide-range XPS spectra of the surfaces of titanium substrate (before) and different unary traisition metal oxides (CoO_x, CuO_x, NiO_x, MnO_x, and FeO_x) before and after the electrochemical oxidation of methane.

Table 4.1. The elemental distributions of blank titanium electrode (before) and different transition metal oxides (CoO_x, CuO_x, NiO_x, FeO_x, and MnO_x) before and after electrochemical oxidation of methane via XPS analysis (Unit: percentage %).

Name	**Titanium**	**CoO_x**		**CuO_x**		**NiO_x**		**MnO_x**		**FeO_x**	
Sample	**Before**	**Before**	**After**	**Before**	**After**	**Before**	**After**	**Before**	**After**	**Before**	**After**
Target element: Ti, Co, Cu, Ni, Mn, or Fe (2p)	Ti: 23.28	Co: 8.59 Ti: 5.24	Co: 9.61 Ti: 0.97	Cu: 26.82 Ti: 0.6	Cu: 6.09 Ti: 0.95	Ni: 14.91 Ti: 3.09	Ni: 15.37 Ti: 2.29	Mn: 20.04	Mn: 12.71	Fe: 22.88	Fe: 21.55
O (1s)	40.4	43.37	40.36	36.36	38.49	44.32	47.91	49.21	33.23	51.43	50.36
C (1s)	35.59	41.41	47.70	35.23	54.46	37.04	33.58	29.2	42.51	25.04	26.89
N (1s)	0.73	0.85	1.12	0.99		0.66	0.34	0.76	0.69	0.65	0.7
Na (1s)		0.24						0.79			
Cl (2p)		0.3	0.24				0.5		0.15		0.5
K (2p)									10.71		

4.2 Electrocatalytic performance for methane partial oxidation

The electrocatalytic activities of different transition metal oxides on electrochemical oxidation of methane were studied in 0.1M K_2CO_3. Figure 4.3 shows the profiles of cyclic voltammetry within specific potential windows on blank titanium cylinder electrode and electrodeposited $CoZrO_x$ onto titanium cylinder electrode for comparison. Although blank titanium already contributes some amount of activity to the methane oxidation reaction in the beginning due to the oxidation reaction of titanium oxides as shown in Figure 4.3. (a), the intrinsic activity is still insignificant compared to electrodeposited $CoZrO_x$. Conversely, in Figure 4.3. (b), the electrocatalytic activities of $CoZrO_x$ have been exhibited under different temperatures. $CoZrO_x$ at room temperature shows higher activity than low temperature (10 ℃). It implies that conducting electrochemical oxidation under low temperature conditions will decrease the overall electrocatalytic activity and may increase the methane solubility in the aqueous electrolyte. Herein, $CoZrO_x$ presents much higher electrocatalytic activity than blank titanium and indicates the electrodeposition method was conducted effectively to enable the electrochemical oxidation of methane.

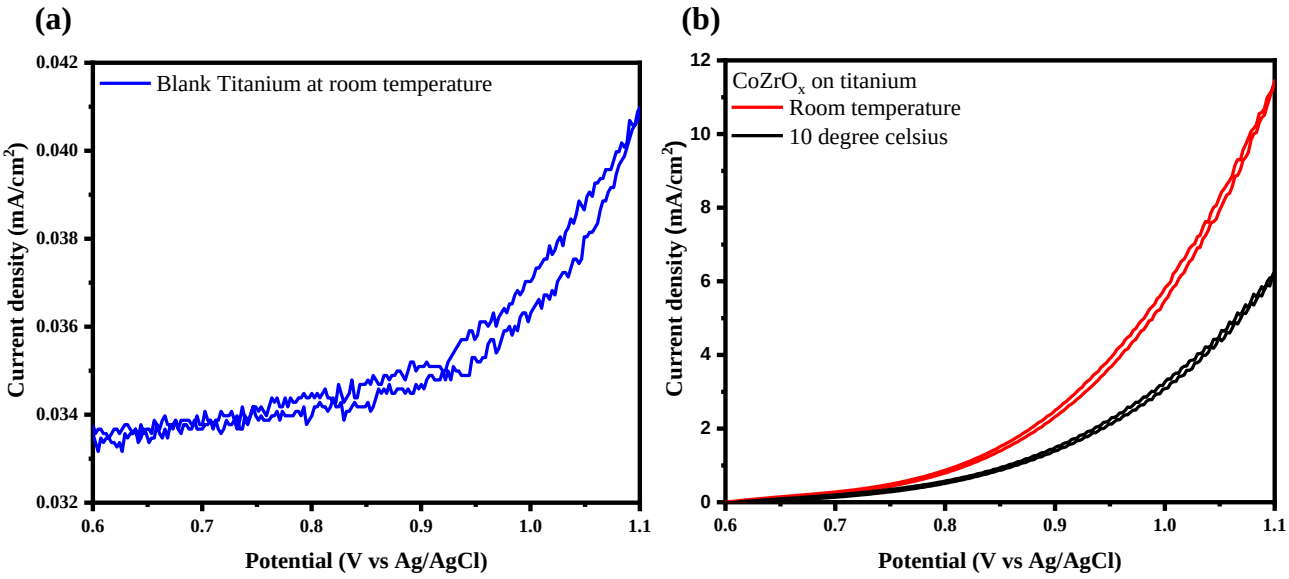

Figure 4.3. Cyclic voltammetry profiles of current density versus potential curves. (a) blank titanium cylinder electrode and (b) electrodeposited $CoZrO_x$ onto titanium cylinder electrode. Conditions: titanium substrate, electrolyte 0.1M K_2CO_3, temperature: 10 °C or room temperature, saturated methane environment, rotational speed: 1600 rpm, and scan rate of 10 mV s^{-1}.

In Figure 4.4, the electrocatalytic activities of different unary transition metal oxides (CoO_x, CuO_x, NiO_x, MnO_x, and FeO_x) is shown under methane saturated environments. CoO_x was found to be the most active among these electrocatalysts and CuO_x is the second most active electrocatalyst. Although NiO_x, MnO_x, and FeO_x were discovered to be less active, their electrocatalytic performances are still higher than blank titanium cylinder electrode which presents a certain amount of materials electrodeposited on the surface of the cylinder electrode. Although MnO_x and FeO_x might possess high catalyst loadings through the electrodeposition of linear sweep voltammetry (Figure A.1), the overall catalytic performances are low compared to NiO_x due to the

non-conductive nature of these materials. [41,48] Overall, different unary transition metal oxides all showed electrocatalytic capabilities for further electrochemical measurements (For details, see the Appendix A. Electrodeposition profiles of different transition metal oxides).

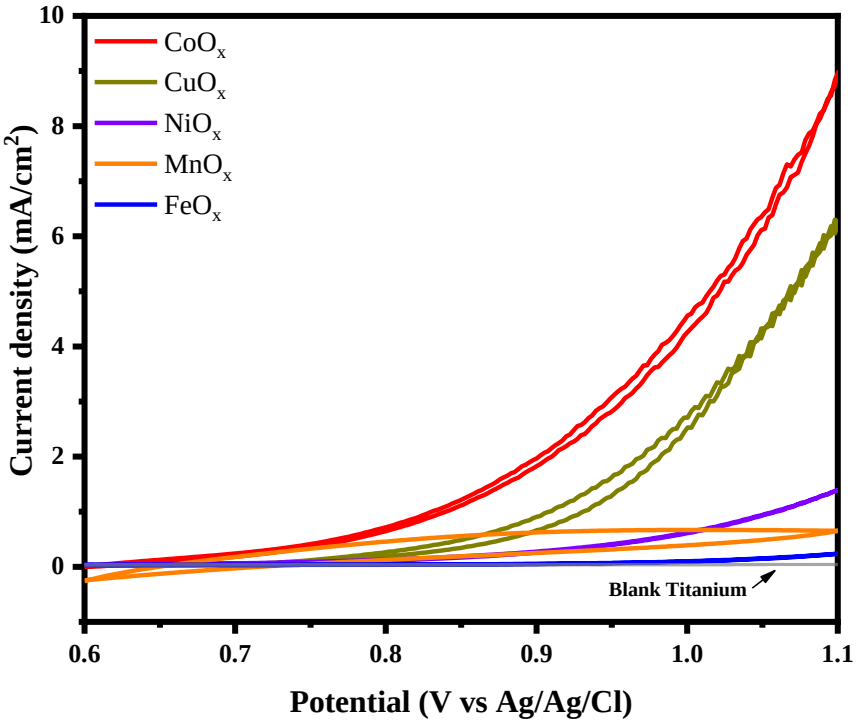

Figure 4.4. Cyclic voltammetry profiles of current density versus potential curves for different transition metal oxides electrodeposited onto titanium cylinder electrode (CoO_x, CuO_x, NiO_x, MnO_x, and FeO_x) showing electrocatalytic performances. Conditions: titanium substrate, electrolyte 0.1M K_2CO_3, room temperature, saturated methane environment, rotational speed: 800 rpm, and scan rate of 10 mV s^{-1}.

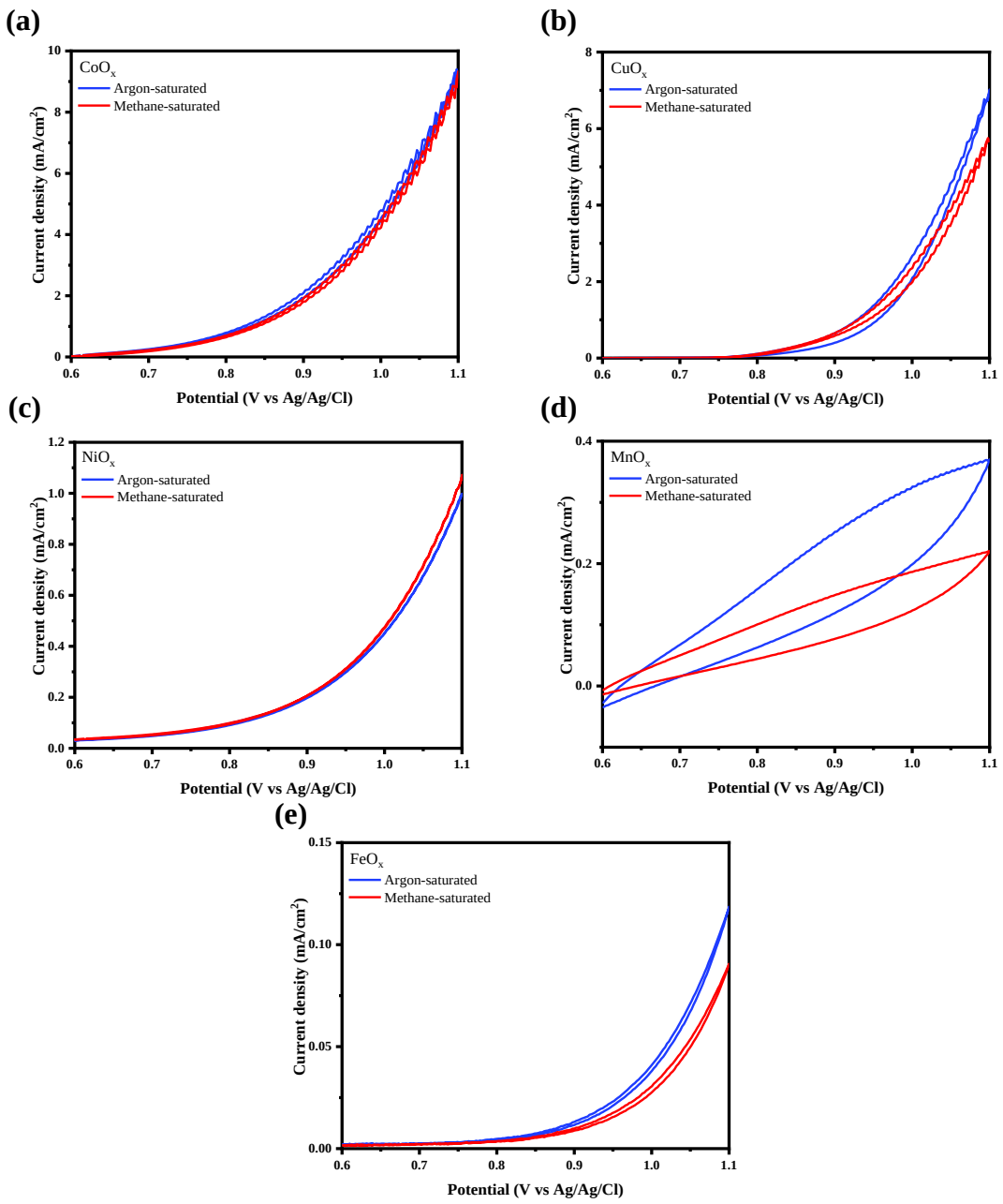

Figure 4.5. Cyclic voltammetry profiles of current density versus potential curves for different electrodeposited transition metal oxides under argon saturated or methane saturated environments. (a) CoO_x (b) CuO_x (c) NiO_x (d) MnO_x and (e) FeO_x. Conditions: titanium substrate, electrolyte 0.1M K_2CO_3, room temperature, saturated environment (argon or methane), rotational speed: 1600 rpm, and scan rate of 10 mV s^{-1}.

As mentioned previously, the different transition metal oxides were prepared by electrodeposition method and their electrocatalytic activities were compared. In the electrochemical measurements of current density versus potential curves (Figure 4.5), an argon saturated environment was used to determine the activity of oxygen evolution reaction (OER) while a methane saturated environment was used to determine the activity of methane oxidation reaction (MOR) competing with OER. Among all unary transition metal oxides as electrocatalysts, CoO_x, CuO_x, and NiO_x were found to be active for the methane oxidation reaction towards methanol (product distribution and analysis will be discussed in the following section 4.3). Since cobalt is a well-known OER electrocatalyst[41], the electrocatalytic performance shows the highest activity in the electrochemical measurement among others. As shown in Figure 4.5. (a), the applied potential above 0.9V is more favorable to OER generating lots of bubbles in the system and leading to the fluctuations in the current at high overpotentials. CoO_x under the methane saturated environment exhibits an analogous phenomenon due to significantly higher activity of OER while methane adsorbed on the surface of the electrode decreases does not affect the activity significantly (Here, $CoZrO_x$ is not included since it shows identical pattern as CoO_x). Similarly, with the presence of the methane saturated environment, CuO_x, MnO_x and FeO_x exhibited decreasing profiles of electrocatalytic activities compared to the Argon saturated environment (Figure 4.5. (b), (d), and (e)). NiO_x, on the other hand, shows much less activity in the system compared to CoO_x and CuO_x. In Figure 4.5. (c), additional electrocatalytic performance under the methane saturated environment suggest that NiO_x may possess the ability of MOR where more catalytic sites might be activated during the electrochemical processes.

4.3 Electrochemical oxidation of methane and product analysis

Figure 4.6. (a) shows the variation of partial current densities (PCD) for MOR towards methanol production at the different applied potentials of $CoZrO_x$ in the carbonate electrolyte conducting one-hour experiments. The decreasing trend of PCD from low to high potentials indicates that MOR at higher potentials might introduce more competing OER and over-oxidize methanol to carbon dioxide. In contrast, MOR at lower potentials could maintain a certain amount of methanol in the electrochemical systems. Figure 4.6. (b) presents the faradaic efficiencies (FEs) for MOR towards methanol at the different applied potentials. FEs at lower potentials (below 0.6V) exceeding 100% implies that some of thermal reactions participate in the overall electrochemical oxidation of methane. In other words, the MOR in the presence of $CoZrO_x$ electrocatalyst is thermodynamically favorable to methanol under atmospheric conditions. As discussed in Figure 4.6, the PCDs at lower potentials have higher values though the FEs are over 100%. Therefore, the $CoZrO_x$ electrocatalyst operating at lower potentials may be sufficiently active and the MOR towards methanol conducting at lower potentials would be more favorable as well.

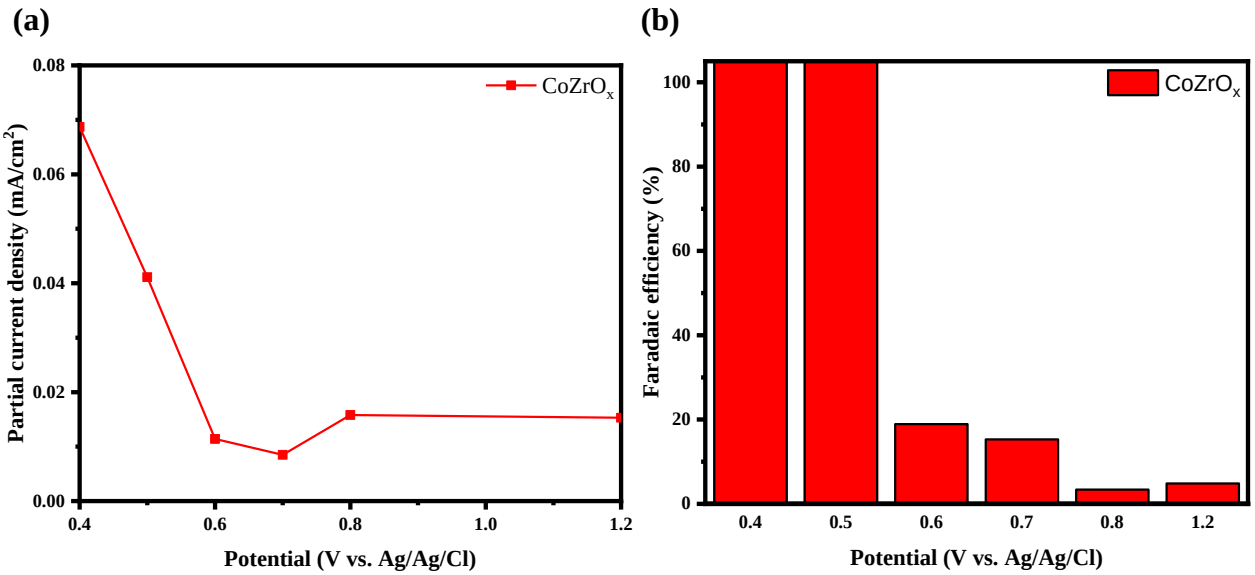

Figure 4.6. (a) Partial current density and (b) faradaic efficiencies of $CoZrO_x$ for electrochemical oxidation of methane reaction producing methanol at different applied potentials 0.4−1.2V vs Ag/AgCl in the carbonate electrolyte for one-hour experiments.

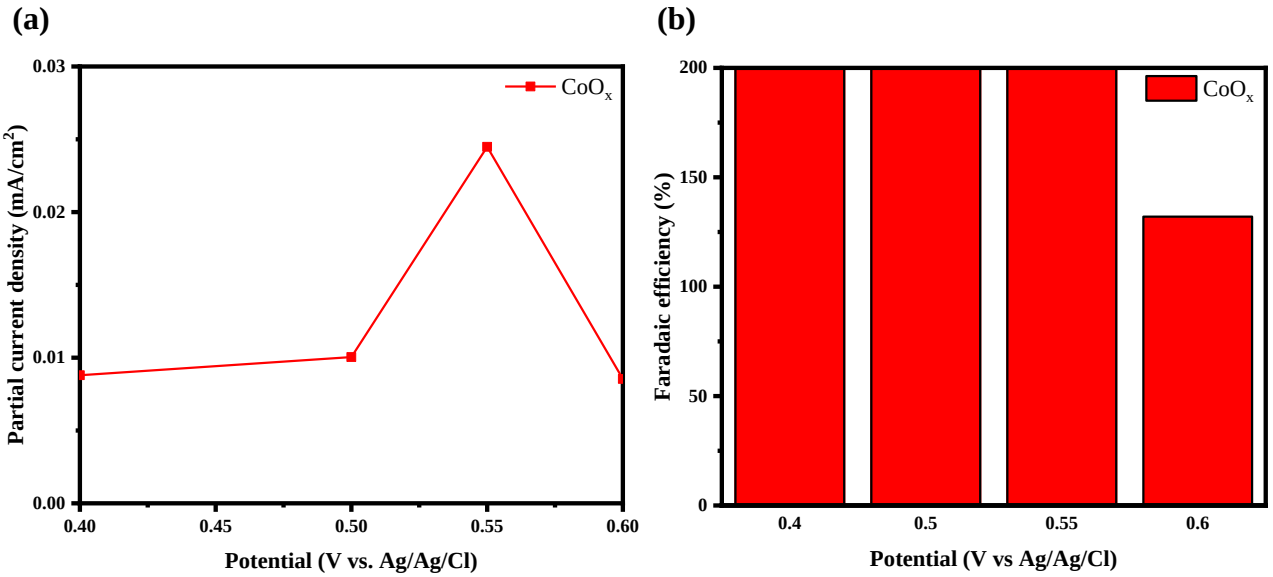

Figure 4.7. (a) Partial current density and (b) faradaic efficiencies of CoO_x for electrochemical oxidation of methane reaction producing methanol at lower applied potentials 0.4−0.6V vs Ag/AgCl in the carbonate electrolyte for one-hour experiments.

Because of the poor reproducibility of $CoZrO_x$ electrocatalyst at lower potentials for the MOR towards methanol, $CoZrO_x$ electrocatalyst was decoupled and unary transition metal oxide (CoO_x) without incorporated zirconia was also studied to determine the ability of cobalt to produce methanol. Figure 4.7 shows the PCDs and FEs for MOR towards methanol production at lower applied potentials (0.4−0.6V) of CoO_x in the carbonate electrolyte conducting one-hour experiments. As shown in Figure 4.7 (a), the CoO_x still has the ability to produce methanol although the PCDs are lower than $CoZrO_x$. Furthermore, the FEs over 100% (FEs at applied potentials below 0.6V are even above 200%) also implies that the CoO_x electrocatalyst is thermodynamically favorable of MOR to methanol under ambient conditions. The methanol production as shown in the trend of PCDs is more stable within the lower potential domain (0.4−0.6V). Consequently, the MOR operating at lower potentials performs better under longer experiments in order to determine the ability of MOR and methanol distribution.

As mentioned before, the MOR operating at lower potentials may obtain higher amount of methanol in the electrochemical oxidation of methane. Nonetheless, considering the open circuit potentials (OCP), typically 0.3−0.4V on average among all the electrocatalysts, and the transient OCPs (0.5−0.55V) after the electrochemical measurements for determination of the electrocatalytic performances at the fixed potential window (0.6−1.1V), two-hours experiments were conducted at the applied potential 0.6V in order to ensure an oxidative state of electrocatalysts to drive MOR towards methanol. Also, the lowest FE at the applied potential 0.6V may contribute more electrochemical reactions in assistance of the overall methane oxidation reaction. As shown in Figure 4.8, the production rate of methanol on CoO_x for the MOR utilized chronoamperometry program operating two-hours experiments under different rotational speeds and samples were taken at different reaction times for NMR product detection. The two-hours experiment under 800

rpm shows the highest production rate: 16.9 μmol h^{-1} while 1600 rpm is the lowest one: 1.7 μmol h^{-1}. On average, the overall production rates within two-hours experiments under 0, 100, 400, 800, and 1600 rpms are 1.065, 1.005, 0, 3.725, and 0.845 μmol h^{-1}, respectively. As discussed earlier, the values of production rate in the beginning (0H) could be thermodynamically favorable MOR in the overall electrochemical reactions because of the participation of thermal reactions and the processes of other electrochemical measurements prior to MOR. Additionally, the negative values of production rate represent the target product methanol being oxidized in the electrochemical system. The production rate under 400 rpm: 0 μmol h^{-1} on average indicates that the amount of methanol produced in the system has been completely oxidized afterwards. Although the CoO_x electrocatalyst is capable of activating methane to methanol, the mass transport and overoxidation issues lead to a fluctuation in the production rate of methanol in the electrochemical system. In theory, high rotational speeds would ameliorate the mass transport limitations and bring more reactants within the boundary layer thickness to proceed MOR. However, in this case, with the use of commercial electrochemical cell, a higher amount of target product methanol is initially produced in the system, and more products would diffuse back and oxidize on the surface of the catalytic electrode. Due to the lower bond dissociation energy (400 kJ mol^{-1}) and polarized molecular structure of methanol compared to methane, methanol is susceptible to overoxidation during the MOR and thus both methane and methanol are present on the electrocatalytic surface and are being oxidized.

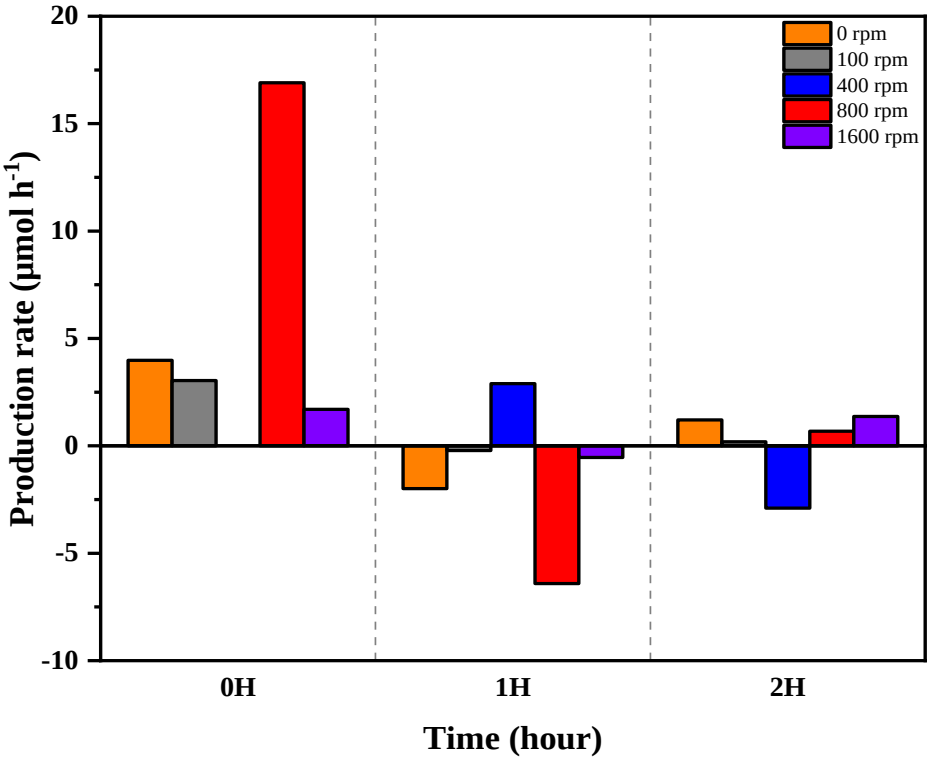

Figure 4.8. The production rate of methanol on CoO_x for electrochemical oxidation of methane reaction at 3 different reaction times within two-hours experiments using the chronoamperometry program performed at 0.6V vs Ag/AgCl under different rotational speeds: 0, 100, 400, 800, and 1600 rpms.

To further study the fluctuation in methanol concentrations and the changes between period of operation where methanol is produced and where methanol is oxidized and its dependence on rotation rates, the production rate of methanol on CoO_x for the MOR was operated in two-hours experiments under different rotational speeds. In these experiments, liquid aliquots were taken at many different reaction times with 20 minutes intervals (Figure 4.9) and analyzed with NMR to quantify products. The experiment under 0 rpm exhibits the highest initial production rate: 12.374 μmol h^{-1} since the reactant of methane adsorbs on the catalytic surface without any mass transport and further oxidize to methanol in the system. Nonetheless, it also shows lowest production rate: −13.7 μmol h^{-1} in the following reaction times due to mass transfer effects of oxidizing methanol subsequently. The experiment under 100 rpm shows the lowest production rate and the ability for activating methane to methanol only presents within the first hour. The experiments under 400 and 800 rpms both show the typically fluctuated distributions of comparable methanol production rate caused by mass transport. On average, the overall production rates within two hours under 0, 100, 400 and 800 rpms are −0.472, −0.16, −0.371, and 0.174 μmol h^{-1}, respectively. With the fundamental understanding of active electrocatalyst CoO_x, it is essential to take mass transfer effects and electrochemical systems into account.

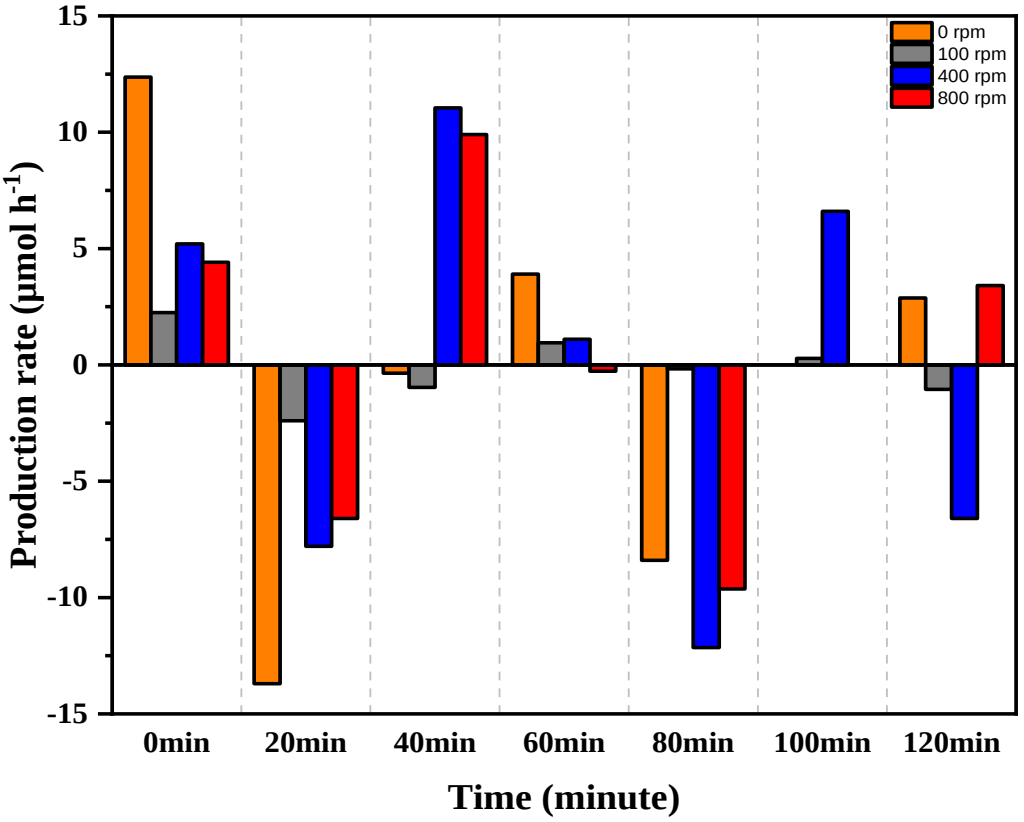

Figure 4.9. The production rate of methanol on CoO_x for electrochemical oxidation of methane reaction at many different reaction times (20 minutes interval) within two-hours experiments using the chronoamperometry program performed at 0.6V vs Ag/AgCl under different rotational speeds: 0, 100, 400, and 800 rpms.

Furthermore, other transition metal oxides (CuO_x, NiO_x, MnO_x, and FeO_x) were investigated for MOR towards methanol. In Figure 4.10, all the electrocatalysts operated two-hours experiments under the same rotational speed: 800 rpm and samples were taken at many different reaction times with 20 minutes intervals. The experiment of NiO_x shows comparable production rate: 11.56 μmol h^{-1} to CoO_x (9.9 μmol h^{-1}) though the electrocatalytic performance is much less active than CoO_x. While CuO_x exhibits second highest electrocatalytic performance over cyclic voltammetry, the production rate: 10.74 μmol h^{-1} is also close to CoO_x and NiO_x. On the other hand, MnO_x and FeO_x could not produce methanol from MOR. Overall, NiO_x and CuO_x are also active to produce methanol and show similar pattern of production distribution as CoO_x due to mass transfer and overoxidation effects in the electrochemical system being dominated entirely by the hydrodynamics in the cell.

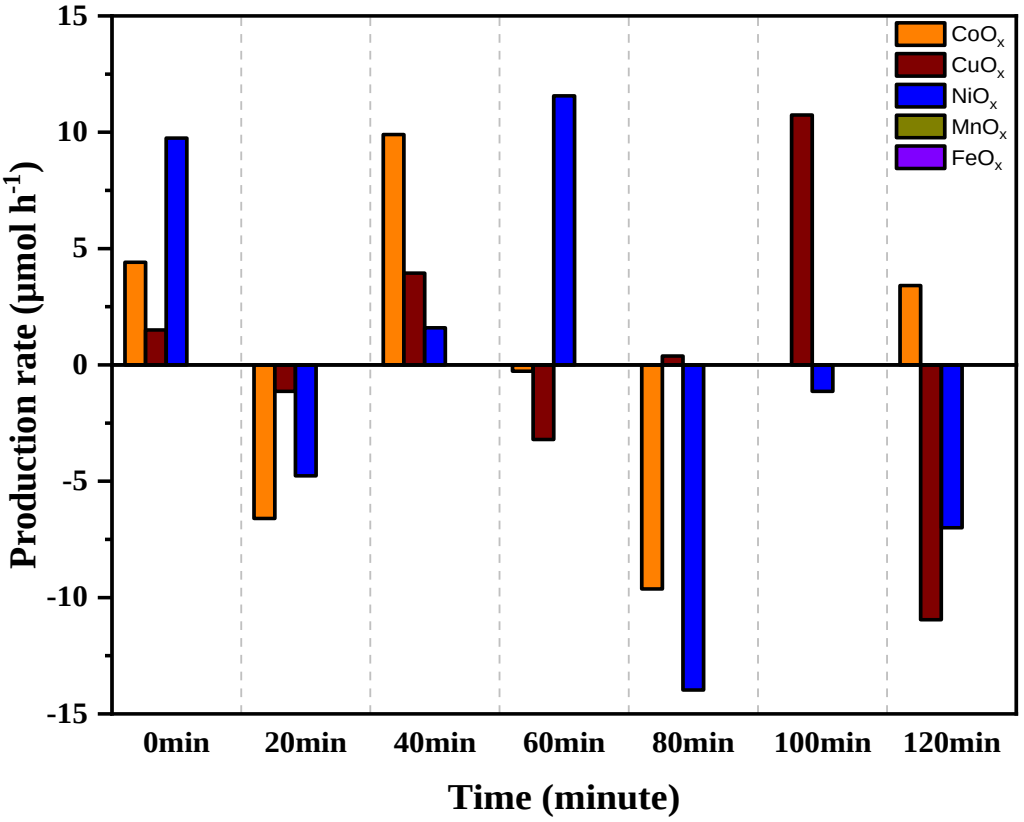

Figure 4.10. The production rate of methanol on different transition metal oxides (CoO_x, CuO_x, NiO_x, MnO_x, and FeO_x) for electrochemical oxidation of methane reaction at many different reaction times (20 minutes interval) within two-hours experiments using the chronoamperometry program performed at 0.6V vs Ag/AgCl under the rotational speeds: 800 rpm.

Among all the electrocatalysts tested over the electrochemical measurements, $CoZrO_x$, CoO_x, NiO_x, and CuO_x were found to be active to produce methanol based on these results. To further clarify the abilities of the MOR towards methanol on these electrocatalysts, the control experiments have been conducted to confirm the active transition metal oxides and the methanol detection (Appendix B). Introducing non-conductive zirconia, participating in the adsorption of carbonate ions, incorporated with cobalt oxide via electrodeposition method to the MOR at ambient temperatures has shown the ability to activate methane towards methanol. Single transition metal oxides prepared through electrodeposition method (CoO_x, NiO_x, and CuO_x) have also shown the ability to activate methane towards methanol where these electrocatalysts have not been investigated the capabilities of methanol production in any other published literatures. MnO_x and FeO_x, on the other hand, show none of results to produce methanol in this study, possibly because they are inactive electrocatalysts that cannot form active oxygen species due to their intrinsically inactive metal oxides and poor conductivity. Based on the fundamental understandings of reaction mechanisms, it is imperative to bridge the reaction mechanisms to electrocatalysis that might be acquired either by oxidants under thermodynamically favorable conditions or electrically driven oxidative potentials. First of all, the dissociation of one of C-H bonds in methane is the primary step for the MOR. The nature of the reaction pathways in the proposed heterogenous reaction systems can be categorized into two types of reaction mechanisms: dehydrogenation and deprotonation. The dehydrogenation mechanism generates adsorbed oxygen atom (O*) by active sites of metal oxides (M-O) involving an abstraction of one of hydrogen atoms (•H) from methane to form the transition states of $\bullet CH_3$ and •OH radicals then the $\bullet CH_3$ radicals react with catalytic surface of •OH sites to produce methanol (Equation 4.1). On the other hand, the deprotonation mechanism decouples methane to CH_3^- and H^+ and CH_3^- subsequently reacts with the

catalytic center to form a M-C bond while H^+ coordinates to the acceptors of surface metals or surface oxygen species in the transition state (Equation 4.2). In this regard, utilizing electrocatalysts may promote surface stabilized M-CH_3 reaction pathway in the C-H bond activation for the production of higher hydrocarbons or oxygenates such as alkanes, alkenes, and alkanols.[2,23,43,44]

$$M - O + CH_4 \rightarrow M - OH + \cdot CH_3 \quad (4.1)$$

$$M + H^+ + CH_4 \rightarrow M - CH_3 + H - H^+ \quad (4.2)$$

Herein, in this work, only the reaction pathway has been considered as the proposed dehydrogenation mechanism for methane to methanol while neglecting any other side reactions and investigating the simple model for the study of activities on the different transition metal oxides. Considering all the possible side reactions, intermediates, and products, the accurate investigation of reaction mechanisms, the rate-limiting steps, and kinetics are indispensable by the studies of theoretical models, practical experiments, and *in situ* characterization. Detailed investigation will not be discussed in this work but it is noteworthy that most of the transition metal oxides are well-know OER electrocatalysts or active for MOR towards methanol and carbon dioxide reactions in all research works. However, the insights of selected electrocatalysts are not well-developed and there is no given rationalization that these electrocatalysts are active for MOR.

5. Conclusion and future expectations

5.1 Conclusion of this work

To summarize, the binary transition metal oxide of $CoZrO_x$ has been fabricated via a one step of electrodeposition method that promotes the MOR to methanol. The $CoZrO_x$ electrocatalyst also shows a mixture of ZrO_x and CoO_x that could be comparable to literature examples of the fabrication of Co_3O_4/ZrO_2 nanocomposite and Co_3O_4 powder/ZrO_2 nanotubes. However, the role of ZrO_2 incorporated with Co_3O_4 remains unclear and the FEs are above 100%, implying that either the chemical reactions might participate between methane and stoichiometric oxidants in the presence of $CoZrO_x$ electrocatalyst or the carbonate electrolyte could be responsible for production of oxygenates. Further studies should investigate the fundamental understandings of kinetics and reaction mechanisms coordinated to zirconia in the electrochemical systems highlighting the formation of methanol (this work) and higher alcohols (other published literatures).

Additionally, the unary transition metal oxides (CoO_x, NiO_x, and CuO_x) have been fabricated effectively and shown the capabilities of methanol production in the commercial electrochemical cell. Due to the mass transfer issue in the commercial cell, the methanol production rates on these electrocatalysts showed fluctuated or irregular patterns on both one-hour experiment and two-hour experiments. With greater amounts of methanol produced in the electrochemical system, greater amounts diffused back and oxidized on the electrocatalytic surface, thus preventing this system from conducting long-term experiments with higher methanol production rates and methane conversion. Based on the fundamental understandings of these active electrocatalysts, it is necessary to take mass transfer effects into account regarding reactant (methane) and product (methanol) transport.

5.2 Future expectations:

5.2.1 Cell design

The prerequisites for electrocatalysts to catalyze methane to methanol are to bring methane onto the active sites with proper orientation to lower activation energy requirement and stimulating oxidation reaction rates, regenerating active oxygen species and preventing overoxidation, and possessing high surface coverage of active sites for electrocatalyst architecture. From the understandings of intrinsic kinetics for electrochemical oxidation of methane, it is essential to bridge these prerequisites to methanol separation, transport, and collection networks.

To fully investigate electrochemical oxidation of methane reaction, the cell design should enhance mass transfer effects of liquid products and compensate missing gaseous products. A gas-tight rotation cell design, that is compatible for RCE, is necessary for further experiments in order to gain fundamental understandings of hydrodynamics and mass transfer effects. The main purpose for the rotation cell is to introduce rotational speeds to the working electrode to reduce boundary layer thickness and eliminate mass transfer limitations. Meanwhile, gaseous products can be quantified in the rotation cell connecting gas inlet and outlet through gas chromatography (GC). Tuning rotational speeds may improve methane oxidation reaction towards methanol and decouple any mass transfer effects of side reactions. Consequently, rotational speeds might be a key factor to determine methane oxidation reaction towards methanol and study the selectivity of methanol and carbon dioxide.

Electrochemical oxidation of methane, typically utilizing water as the oxidant in aqueous electrolyte, indicates that it may be possible to attain the high selectivity of methanol at certain conversion levels by applying an appropriate electrocatalyst. However, high selectivity of methanol usually undergoes low methane conversions that brings the other challenge conducting

on the overall methane oxidation reaction. While using aqueous electrolyte may be useful to obtain high sensitivity product detection, it could not overcome this challenge due to poor mass transfer and low solubility of methane. Therefore, methanol separation, transport, and collection are a major concern in the systems since our target product may encounter overoxidation. In this regard, an electrochemical system, membrane electrode assembly (MEA) including vapor fed and aqueous electrolyte solution fed on both sides of the cells, has been proposed to explore electrochemical oxidation of methane to methanol for regulating the local pH and microenvironment within boundary layer thickness. The primary characteristic of the MEA architecture is to render reactant and product transport more efficiently on the electrocatalytic surface and to minimize ohmic loss through the membrane (ion-conducting medium). The utilization of MEA on the methanol production is promising because it provides advanced orientation through the electrocatalytic microenvironment and selective transport between reactants and products. Julie C. Fornaciari et al have reported that MEA may introduce new insights to address the issues related to high selectivity with low conversion since current electrochemical systems are still struggling to overcome these challenges due to required low over potentials to minimize overoxidation and maximize selectivity.[43]

5.2.2 Catalyst characterization

The different transition metal oxides need to be studied comprehensively throughout the electrodeposition method including single metal oxide or combinations of two or three metal oxides such as ZrO_2/Co_3O_4, ZrO_2/NiO, and $ZrO_2/NiCo_2O_4$ in order to explore the capabilities of methanol selectivity and the production of higher oxygenates or hydrocarbons. Furthermore, it is indispensable that the study of electrochemical interface sheds the light on reaction mechanisms and intermediates on the electrocatalytic surface over *in situ* techniques such as Fourier transform

infrared spectroscopy (FTIR) and Raman spectroscopy. Advanced tools for *in situ* observation are motivated in order to gain useful experimental results. Additionally, X-ray absorption/diffraction has shown that *in situ* monitoring of electrocatalysts can be applied to explore electrodeposited materials at a deeper atomic level such as chemical oxidation state, coordination environment, and crystal nature. More *in situ* experiments should be effectively demonstrated to capture the reaction intermediates and to better understand the reaction mechanisms and the behaviors of active sites more precisely.[45–47]

For further practical applications, significant catalyst loadings are vital to maintain relatively low overpotential particularly for high current density (0.5−2 A cm^{-2}) of electrolyzers in larger scale processes.[43] Catalyst loadings will be a significant factor to investigate the relationship between loading and activity on the methane oxidation reaction. Systematic studies are necessary to quantify the combination of electrodeposited transition metal oxides through quartz crystal microbalance (QCM). The extended transition metal oxides of catalyst loadings may be dependent of activity of methane oxidation reaction reflecting the reaction turnover frequency (TOF).[41]

Appendices

Appendix A. Electrodeposition profiles

In the electrodeposition process, most electrocatalysts ($CoZrO_x$, CoO_x, NiO_x, MnO_x, and FeO_x) were electrodeposited by 100 cycles of consecutive linear sweeps within the potential window through linear sweep voltammetry program while copper oxide (CuO_x) was obtained by applying constant potential via chronoamperometry program (Figure A.1).

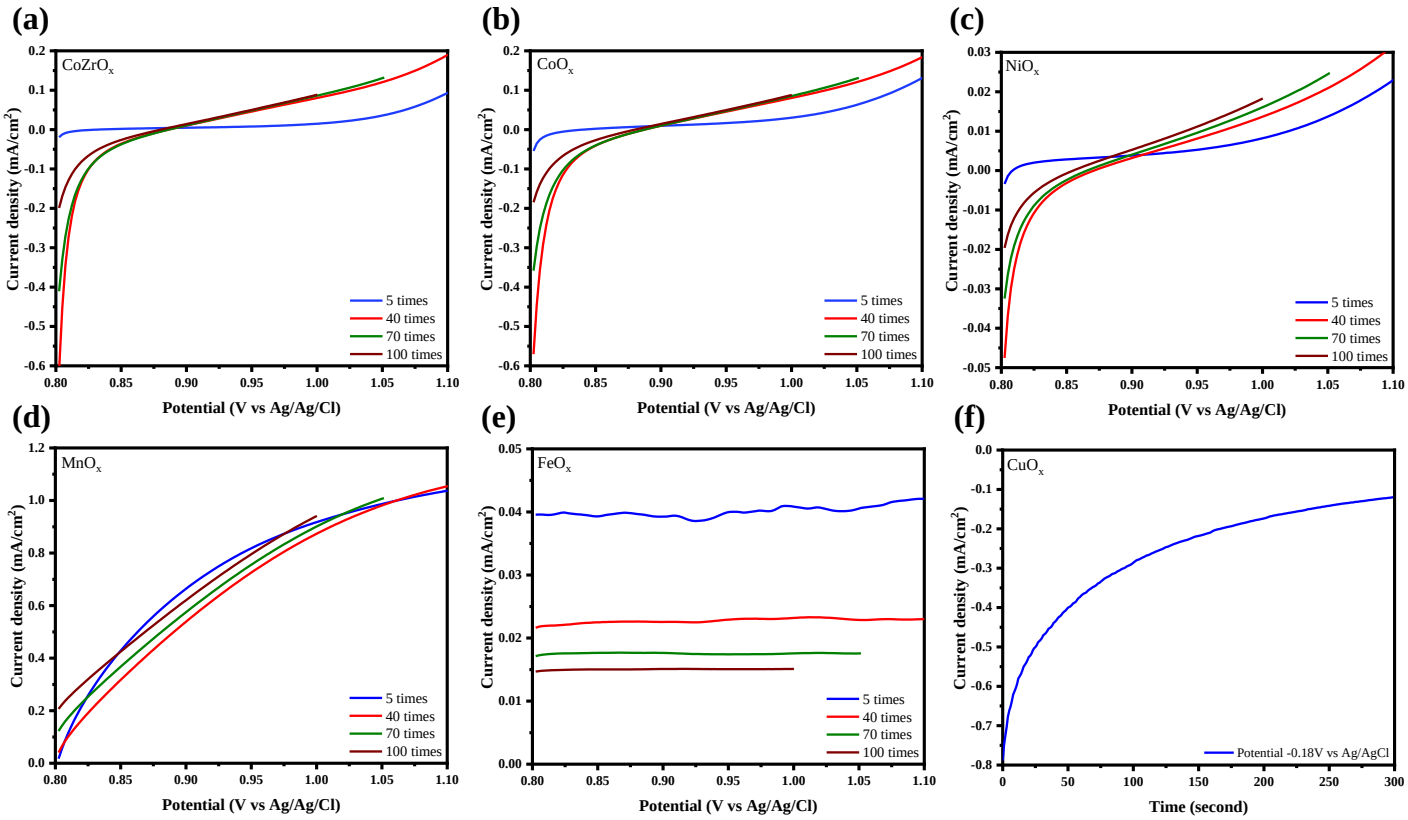

Figure A.1. The electrodeposition profiles of different transition metal oxides via the programs of linear sweep voltammetry (a) $CoZrO_x$, (b) CoO_x (c) NiO_x (d) MnO_x and (e) FeO_x and chronoamperometry (f) CuO_x. All the electrodeposition processes conducted in the bath of 0.1 M sodium under ambient conditions.

Appendix B. Control experiments

Nuclear Magnetic Resonance (NMR) Spectroscopy (1D ^{1}H-NMR spectroscopy) was performed to quantitatively determine the presence of methanol as the MOR product for active electrocatalysts ($CoZrO_x$, CoO_x, NiO_x, and CuO_x). The blank titanium cylinder electrode was used as the control experiment followed by the same electrochemical measurements to confirm the NMR's capability of methanol detection and blank titanium is inactive to produce methanol (Figure B.1). Furthermore, the active electrocatalyst (CoO_x and NiO_x) were conducted under inert gas (argon saturated environment) as the control experiment followed by the same electrochemical measurements in the identical manner of methanol detection (Figure B.2). In the following Figure B.3, the production distribution has shown only little amount of acetate in the system under argon saturated environment. Lastly, the dissolution samples of CoO_x electrocatalyst was prepared to determine the possible contaminants from the catalyst preparation. In Figure B.4, the preparation of dissolution samples was followed by dissolving CoO_x electrocatalyst in the several droplets (2−3 ml) of 2 M hydrochloric acid after the electrodeposition process, then added 0.1 M potassium carbonate electrolyte to 100 ml, and stirred and mixed well the solution followed by samples taken for NMR detection. As shown in Figure B.4, the results indicate that some amount of acetate (below 5 μM) is unavoidable in the electrochemical systems since the experiments were conducted by using acetate species in the electrodeposition bath though the concentration of acetate is trivial. Its concentration is also independent of methanol production and there is no methanol shown in the NMR spectra from the dissolution experiments.

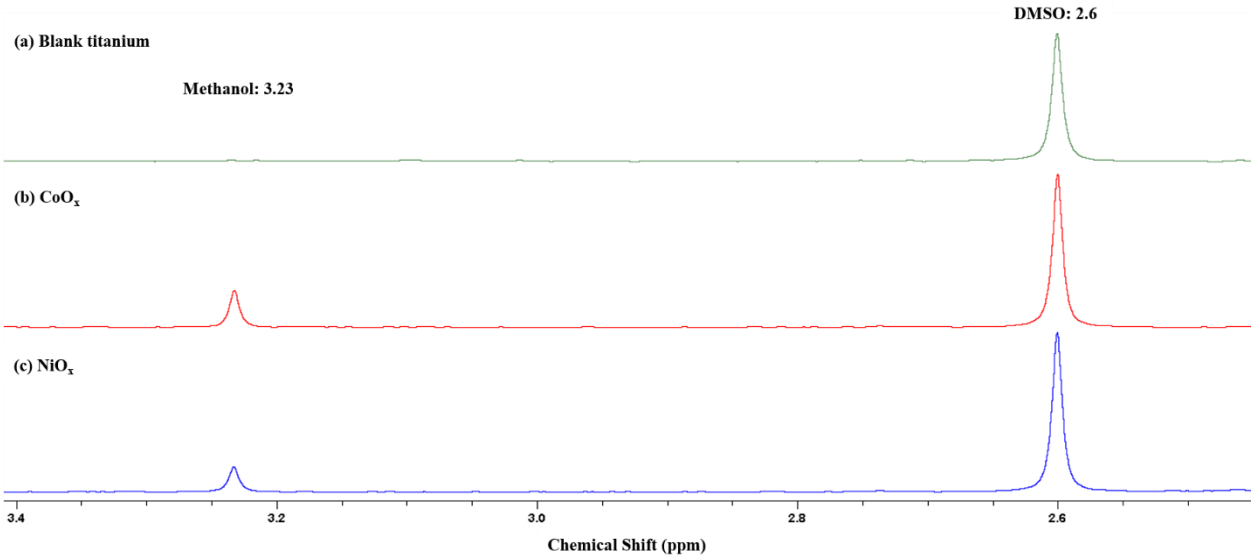

Figure B.1. 1D ^{1}H-NMR spectra of methanol chemical shift with (a) blank titanium cylinder electrode (green), (b) CoO_x (red), and (c) NiO_x (blue) under methane saturated environment after the chronoamperometry program performed at 0.6V vs Ag/AgCl.

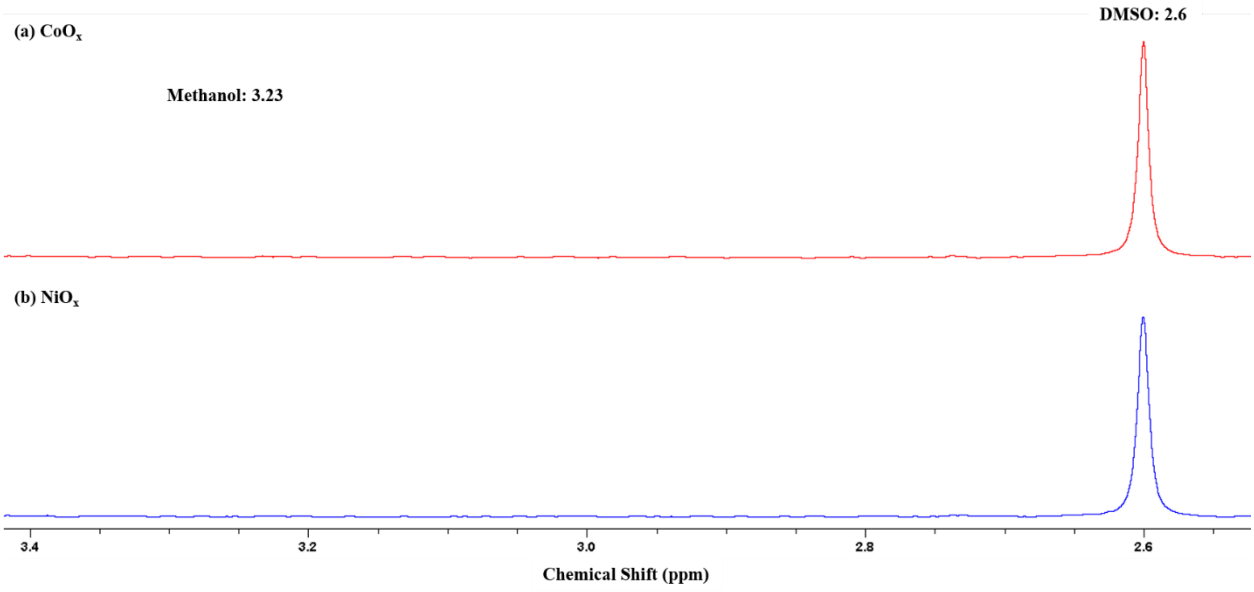

Figure B.2. 1D ^{1}H-NMR spectra of methanol chemical shift with (a) CoO_x (red), and (b) NiO_x (blue) under argon saturated environment after the chronoamperometry program performed at 0.6V vs Ag/AgCl.

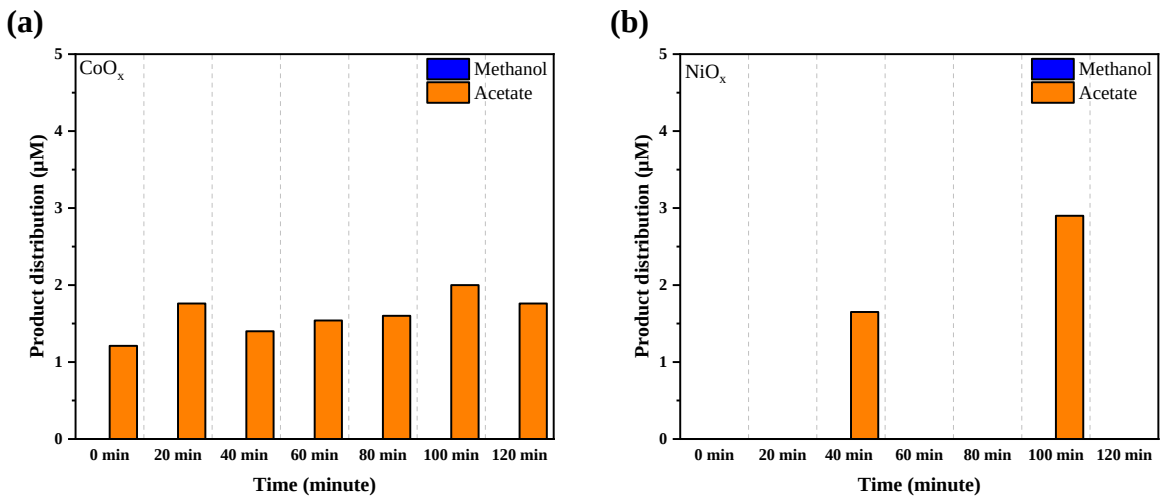

Figure B.3. Product distribution on (a) CoO_x and (b) NiO_x under argon saturated environment at many different reaction times (20 minutes interval) within two-hours experiments using the chronoamperometry program performed at 0.6V vs Ag/AgCl under the rotational speeds: 800 rpm.

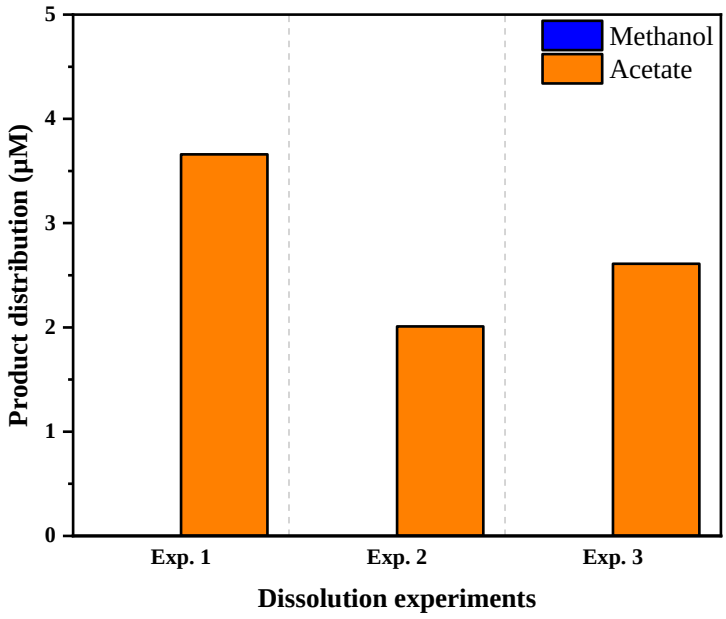

Figure B.4. The amount of methanol and acetate in the prepared dissolution experiments from the electrodeposited CoO_x catalyst.

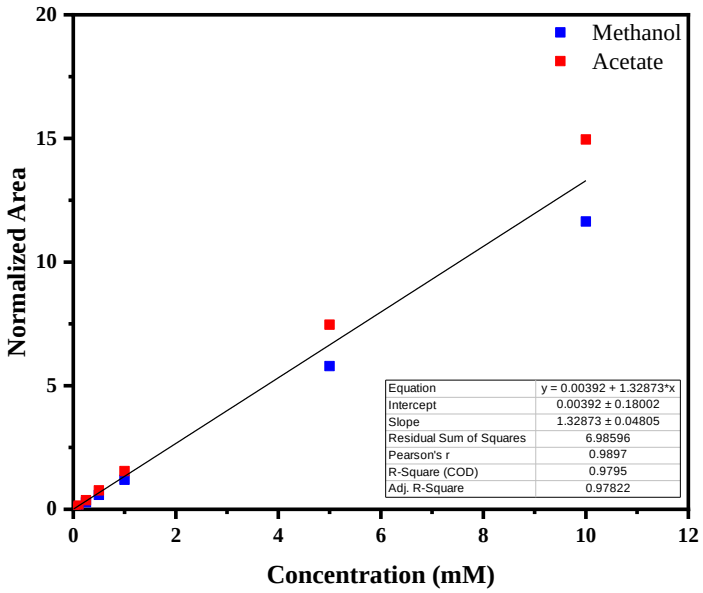

Figure B.5. Calibration curve for methanol and acetate normalized by relative area and number of protons detected from external standard products (methanol and acetate) with concentrations of 0.01, 0.05, 0.1, 0.25, 0.5, 1, 5, and 10 mM through the quantification of NMR spectra.

Appendix C. Supplementary information

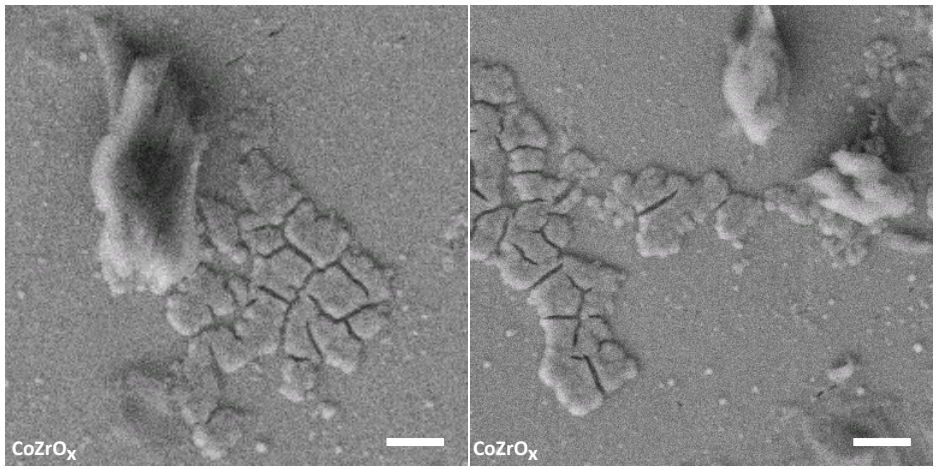

Figure C.1. SEM images of $CoZrO_x$ present zirconium co-electrodeposited with cobalt oxide onto the titanium cylinder electrode. The scale bars in these samples are 1 μm.

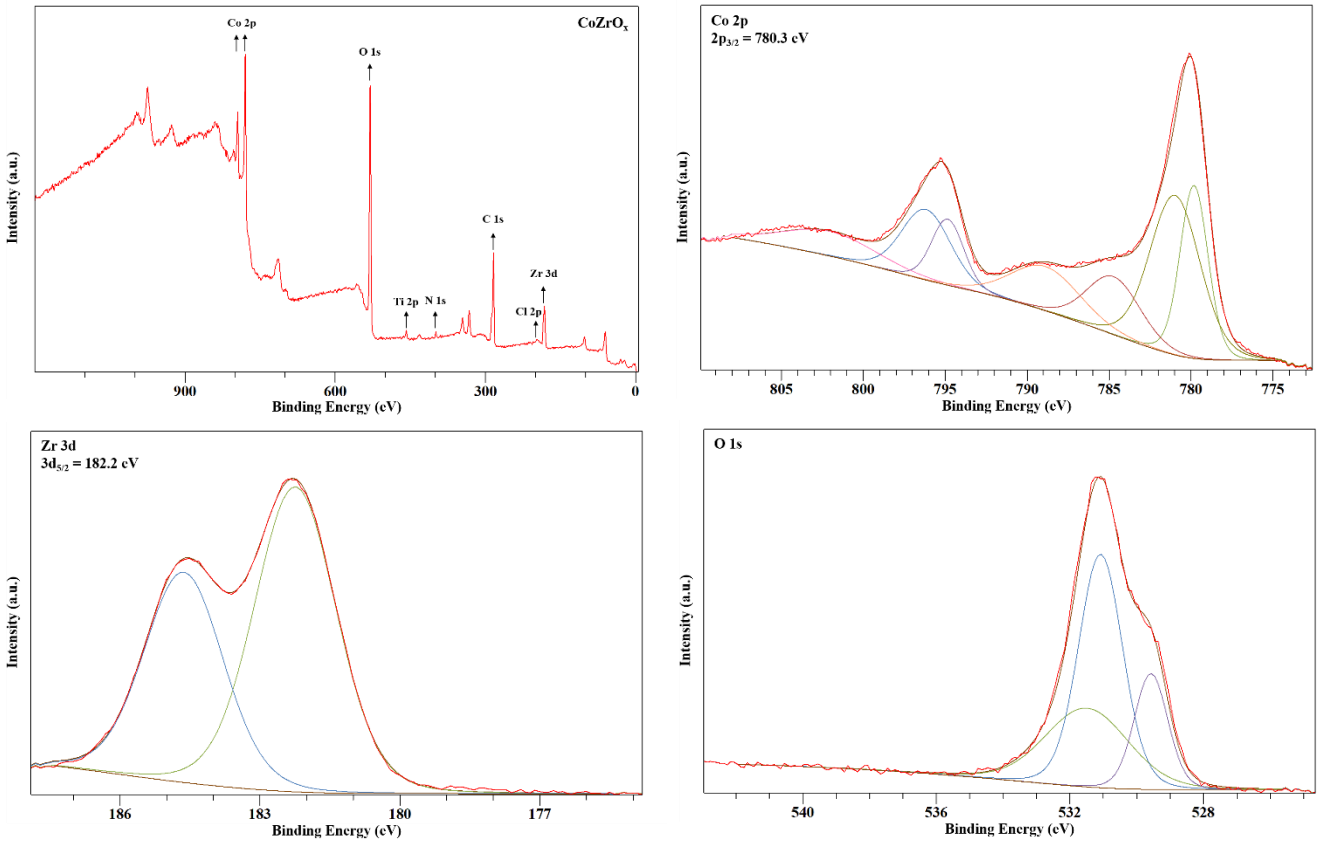

Figure C.2. Wide-range, Co 2p, Zr 3d, and O 1s of the XPS spectra for $CoZrO_x$.

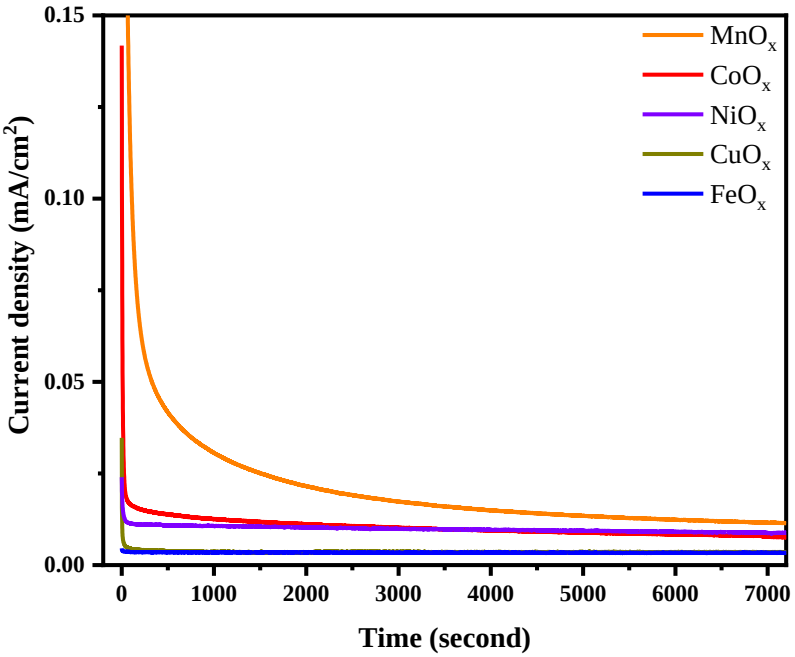

Figure C.3. The profiles of chronoamperometry for two-hours electrochemical oxidation of methane on different transition metal oxides performed at 0.6V vs Ag/AgCl under the rotational speeds: 800 rpm.

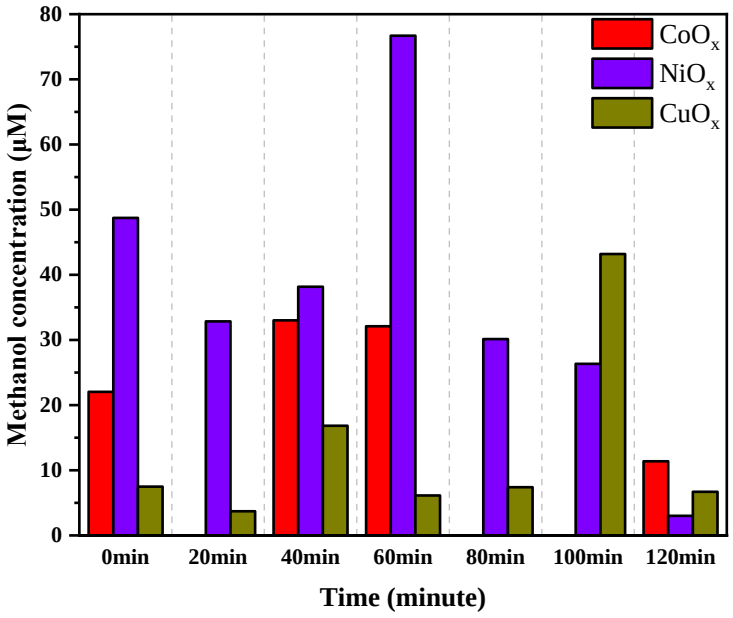

Figure C.4. The amount of methanol concentrations on CoO_x, NiO_x, and CuO_x at many different reaction times (20 minutes interval) within two-hours experiments using the chronoamperometry program performed at 0.6V vs Ag/AgCl under the rotational speeds: 800 rpm.

References

1. Levi, P. G. & Cullen, J. M. Mapping Global Flows of Chemicals: From Fossil Fuel Feedstocks to Chemical Products. *Environmental Science and Technology* **52**, 1725–1734 (2018).

2. Yuan, S. *et al.* Conversion of Methane into Liquid Fuels—Bridging Thermal Catalysis with Electrocatalysis. *Advanced Energy Materials* vol. 10 (2020).

3. Energy Information Administration, U.S. *Annual Energy Outlook 2021 Narrative*. https://www.eia.gov/outlooks/aeo/

4. *Global Gas Flaring Tracker Report JULY 2020 Global Gas Flaring Reduction Partnership*. (2020).

5. Tracking Industry 2020 – Analysis - IEA. https://www.iea.org/reports/tracking-industry-2020

6. Energy Transitions Commission, Mission Possible: Reaching net-zero carbon emissions from harder-to-abate sectors by mid-century,2018 http://www.energy-transitions.org/mission-possible,

7. Keith, D. W., Holmes, G., st. Angelo, D. & Heidel, K. A Process for Capturing CO2 from the Atmosphere. *Joule* **2**, 1573–1594 (2018).

8. Falter, W., Langer, A., Wesche, F. & Wezel, S. Practitioner's Section Decarbonization strategies in converging chemical and energy markets. *Journal of Business Chemistry* **2020**, 20.

9. Welborn, V. V., Ruiz Pestana, L. & Head-Gordon, T. Computational optimization of electric fields for better catalysis design. *Nature Catalysis* vol. 1 649–655 (2018).

10. Arnarson, L. *et al.* Fundamental limitation of electrocatalytic methane conversion to methanol. *Physical Chemistry Chemical Physics* **20**, 11152–11159 (2018).

11. Baba, T. & Miyaji, A. *Catalysis and the mechanism of methane conversion to chemicals: C-C and C-O bonds formation using heterogeneous, homogenous, and biological catalysts*. *Catalysis and the Mechanism of Methane Conversion to Chemicals: C-C and C-O Bonds Formation Using Heterogeneous, Homogenous, and Biological Catalysts* (Springer Singapore, 2020). doi:10.1007/978-981-15-4132-2.

12. Bagherzadeh Mostaghimi, A. H., Al-Attas, T. A., Kibria, M. G. & Siahrostami, S. A review on electrocatalytic oxidation of methane to oxygenates. *Journal of Materials Chemistry A* vol. 8 15575–15590 (2020).

13. Jang, J., Shen, K. & Morales-Guio, C. G. Electrochemical Direct Partial Oxidation of Methane to Methanol. *Joule* **3(11)**, 2589-2593 (2019).

14. Dalton, H. The Leeuwenhoek Lecture 2000 The natural and unnatural history of methane-oxidizing bacteria. *Philosophical Transactions of the Royal Society B: Biological Sciences* **360**, (2005).

15. Lee, S. J., McCormick, M. S., Lippard, S. J. & Cho, U. S. Control of substrate access to the active site in methane monooxygenase. *Nature* **494**, 380–384 (2013).

16. Banerjee, R., Jones, J. C. & Lipscomb, J. D. Soluble Methane Monooxygenase. *Annual Review of Biochemistry* **88**, (2019).

17. Khokhar, M. D., Shukla, R. S. & Jasra, R. v. Selective oxidation of methane by molecular oxygen catalyzed by a bridged binuclear ruthenium complex at moderate pressures and ambient temperature. *Journal of Molecular Catalysis A: Chemical* **299**, (2009).

18. Shilov, A. E. & Shul'pin, G. B. Activation of C−H Bonds by Metal Complexes. *Chemical Reviews* **97**, (1997).

19. Dinh, K. T. *et al.* Viewpoint on the Partial Oxidation of Methane to Methanol Using Cu- and Fe-Exchanged Zeolites. *ACS Catalysis* **8**, (2018).

20. Hammond, C. *et al.* Direct Catalytic Conversion of Methane to Methanol in an Aqueous Medium by using Copper-Promoted Fe-ZSM-5. *Angewandte Chemie* **124**, (2012).

21. Horn, R. & Schlögl, R. Methane Activation by Heterogeneous Catalysis. *Catalysis Letters* **145**, 23–39 (2015).

22. Catalytic Oxidation of Methane to Oxygenated Products Recent Advancements and Prospects for Electrocatalytic and Photocatalytic Conversion at Low Temperatures.

23. Latimer, A. A., Kakekhani, A., Kulkarni, A. R. & Nørskov, J. K. Direct Methane to Methanol: The Selectivity-Conversion Limit and Design Strategies. *ACS Catalysis* **8**, 6894–6907 (2018).

24. Spinner, N. & Mustain, W. E. Electrochemical Methane Activation and Conversion to Oxygenates at Room Temperature. *Journal of The Electrochemical Society* **160**, F1275–F1281 (2013).

25. Jocz, J. N., Medford, A. J. & Sievers, C. Thermodynamic Limitations of the Catalyst Design Space for Methanol Production from Methane. *ChemCatChem* **11**, 593–600 (2019).

26. Alexiadis, V. I. *et al.* Oxidative coupling of methane: catalytic behaviour assessment via comprehensive microkinetic modelling. *Applied Catalysis B: Environmental* **150–151**, (2014).

27. Choudhary, T. v., Aksoylu, E. & Wayne Goodman, D. Nonoxidative Activation of Methane. *Catalysis Reviews* **45**, (2003).

28. Malerød-Fjeld, H. *et al.* Thermo-electrochemical production of compressed hydrogen from methane with near-zero energy loss. *Nature Energy* **2**, 923–931 (2017).

29. Kyriakou, V., Garagounis, I., Vourros, A., Vasileiou, E. & Stoukides, M. An Electrochemical Haber-Bosch Process. *Joule* **4**, (2020).

30. Garagounis, Vourros, Stoukides, Dasopoulos & Stoukides. Electrochemical Synthesis of Ammonia: Recent Efforts and Future Outlook. *Membranes* **9**, (2019).

31. Deng, J. *et al.* Ambient methane functionalization initiated by electrochemical oxidation of a vanadium (V)-oxo dimer. *Nature Communications* **11**, (2020).

32. Ma, M. *et al.* Ultrahigh Electrocatalytic Conversion of Methane at Room Temperature. *Advanced Science* **4**, (2017).

33. Omasta, T. J. *et al.* Two Pathways for Near Room Temperature Electrochemical Conversion of Methane to Methanol. *ECS Transactions* **66**, 129–136 (2015).

34. Oh, C., Kim, J., Hwang, Y. J., Ma, M. & Park, J. H. Electrocatalytic methane oxidation on Co3O4- incorporated ZrO2 nanotube powder. *Applied Catalysis B: Environmental* **283**, (2021).

35. Prajapati, A., Collins, B. A., Goodpaster, J. D. & Singh, M. R. Fundamental insight into electrochemical oxidation of methane towards methanol on transition metal oxides. *Proceedings of the National Academy of Sciences* **118**, (2021).

36. Rocha, R. S., Reis, R. M., Lanza, M. R. V. & Bertazzoli, R. Electrosynthesis of methanol from methane: The role of V2O5 in the reaction selectivity for methanol of a TiO2/RuO2/V2O5 gas diffusion electrode. *Electrochimica Acta* **87**, (2013).

37. Guo, Z. *et al.* Efficient methane electrocatalytic conversion over a Ni-based hollow fiber electrode. *Chinese Journal of Catalysis* **41**, (2020).

38. Song, Y. *et al.* Electrocatalytic oxidation of methane to ethanol via NiO/Ni interface. *Applied Catalysis B: Environmental* **270**, (2020).

39. Ma, M., Oh, C., Kim, J., Moon, J. H. & Park, J. H. Electrochemical CH4 oxidation into acids and ketones on ZrO2:NiCo2O4 quasi-solid solution nanowire catalyst. *Applied Catalysis B: Environmental* **259**, (2019).

40. Kim, R. S. & Surendranath, Y. Electrochemical Reoxidation Enables Continuous Methane-to-Methanol Catalysis with Aqueous Pt Salts. *ACS Central Science* **5**, (2019).

41. Morales-Guio, C. G., Liardet, L. & Hu, X. Oxidatively Electrodeposited Thin-Film Transition Metal (Oxy)hydroxides as Oxygen Evolution Catalysts. *Journal of the American Chemical Society* **138**, (2016).

42. *Study of Mass Transport Limited Corrosion with Rotating Cylinder Electrodes*. (2008).

43. Fornaciari, J. C. *et al.* A Perspective on the Electrochemical Oxidation of Methane to Methanol in Membrane Electrode Assemblies. *ACS Energy Letters* **5**, (2020).

44. Latimer, A. A. *et al.* Mechanistic insights into heterogeneous methane activation. *Physical Chemistry Chemical Physics* **19**, 3575–3581 (2017).

45. Zhang, M., de Respinis, M. & Frei, H. Time-resolved observations of water oxidation intermediates on a cobalt oxide nanoparticle catalyst. *Nature Chemistry* **6**, 362–367 (2014).

46. Diaz-Morales, O., Ferrus-Suspedra, D. & Koper, M. T. M. The importance of nickel oxyhydroxide deprotonation on its activity towards electrochemical water oxidation. *Chemical Science* **7**, (2016).

47. Trześniewski, B. J. *et al.* In Situ Observation of Active Oxygen Species in Fe-Containing Ni-Based Oxygen Evolution Catalysts: The Effect of pH on Electrochemical Activity. *Journal of the American Chemical Society* **137**, (2015).

48. Burke, M. S., Enman, L. J., Batchellor, A. S., Zou, S., & Boettcher, S. W. Oxygen evolution reaction electrocatalysis on transition metal oxides and (oxy) hydroxides: activity trends and design principles. *Chemistry of Materials* **27(22)**, 7549-7558 (2015).